

# *Techniques for understanding fold-and-thrust belt kinematics and thermal evolution*

**Nadine McQuarrie**

*Department of Geology and Environmental Science, University of Pittsburgh, Pittsburgh, Pennsylvania 15260, USA*

**Todd A. Ehlers**

*Department of Geoscience, University of Tübingen, Tübingen 72074, Germany*

## ABSTRACT

**Fold-and-thrust belts and their adjacent foreland basins provide a wealth of information about crustal shortening and mountain-building processes in convergent orogens. Erosion of the hanging walls of these structures is often thought to be synchronous with deformation and results in the exhumation and cooling of rocks exposed at the surface. Applications of low-temperature thermochronology and balanced cross sections in fold-and-thrust belts have linked the record of rock cooling with the timing of deformation and exhumation. The goal of these applications is to quantify the kinematic and thermal history of fold-and-thrust belts. In this review, we discuss different styles of deformation preserved in fold-and-thrust belts, and the ways in which these structural differences result in different rock cooling histories as rocks are exhumed to the surface. Our emphasis is on the way in which different numerical modeling approaches can be combined with low-temperature thermochronometry and balanced cross sections to resolve questions surrounding the age, rate, geometry, and kinematics of orogenesis.**

## INTRODUCTION

Folding and thrust faulting are the primary mechanisms for the shortening and thickening of continental crust and thus are common geologic features of convergent margins. Previous work has clearly documented that crustal shortening produces a distinctive suite of structures, including faults that extend both parallel to bedding and across it, and the resulting folds produced by motion on the faults (e.g., Rich, 1934; Dahlstrom, 1969; Boyer and Elliott, 1982; McClay, 1992). Examples include duplexes and imbricate faults, which form as a result of an inherent mechanical anisotropy in stratigraphic layers. Because of this link between fold-and-thrust belts and mechanical anisotropy, a precondition

for fold-and-thrust belt formation is an extensive preexisting sedimentary basin of platformal to passive-margin strata (Fig. 1). The mechanical anisotropy of stratigraphic layering exerts a first-order control on the style and magnitude of shortening (Price, 1981; Stockmal et al., 2007). The large magnitude of convergence accommodated by fold-and-thrust belts produces some of the largest mountains in the world, such as the Central Andean thrust belt (eastern Peru, Bolivia, and Argentina) and the southern flank of the Himalaya. Furthermore, crustal thickening due to structural repetition and the burial of rocks due to sedimentation lead to the creation of natural hydrocarbon traps that host a large percentage of the world's oil and gas reserves. An understanding of the geometry and kinematics of fold-and-thrust belt systems

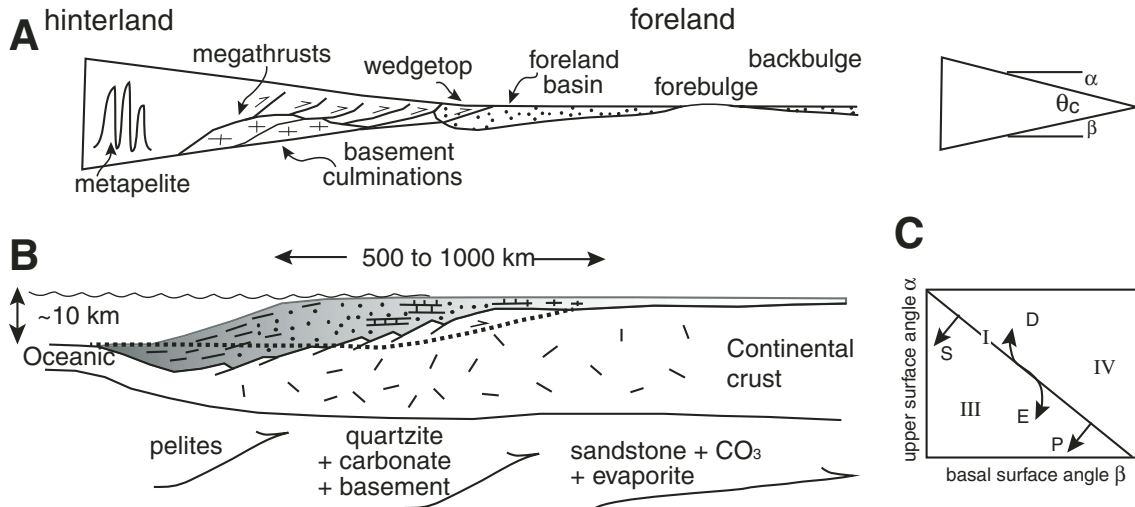


Figure 1. (A) Schematic diagram of a critical wedge geometry, highlighting locations of major fold-and-thrust belt structure (P.G. DeCelles, 2000, personal commun.).  $\theta_c$  is critical wedge,  $\alpha$  is the topographic slope, and  $\beta$  is the basal décollement. (B) Schematic passive-margin geometry, depicting original sedimentary basin taper and distribution of typical sedimentary rocks. (C) Behavior of Coulomb wedge in  $\alpha$ - $\beta$  space in response to changing key parameters (modified from DeCelles and Mitra, 1995). I—critical wedge, wedge advances in self-similar form; III—subcritical wedge, the wedge does not advance but deforms internally to regain taper; IV—supercritical wedge, structure promotes normal faulting or forward propagation to regain critical taper; S—increase in wedge strength, P—increase in pore pressure or decrease in basal strength, D—increase in durability of the surface, E—erosion of the surface.

is a requirement for understanding how these mountains and natural reservoirs form. Fold-and-thrust belts provide a record of the amount of continental crustal shortening and thus provide an estimate of the amount of plate convergence absorbed by continents. If the magnitude of crustal shortening can be tied to age constraints on deformation and deformation-related denudation, then fold-and-thrust belt systems provide a record of the ways in which the magnitude and rate of deformation have evolved with time, allowing us to evaluate the driving processes behind deformation. In this review, we focus our discussion on the ways in which knowledge of the thermal evolution of a fold-and-thrust belt (via thermochronology) can aid in constraining the deformation history.

Deformation, denudation, and sedimentation associated with fold-and-thrust belts can exert a large influence on the thermal state of continental crust and the lithosphere. The structural development and denudation of a fold-and-thrust belt modify the subsurface thermal field by producing lateral variations in the depth to a given isotherm. This is particularly true for upper-crustal ( $< \sim 15$  km) temperatures, where stacking of thrust sheets, denudation, and topographic effects on isotherms are the largest (e.g., Mancktelow and Graseman, 1997; Stuwe et al., 1994; Rahn and Grasemann, 1999; Olen et al., 2012). As thrust faults propagate and move upward along footwall ramps, the vertical component of motion and the exhumation advect heat upward. The upward motion creates topography and focuses erosion, and the upward advection of isotherms is enhanced (Shi and Wang, 1987; Huerta et al., 1996; Rahn and Grasemann, 1999; Ehlers and Far-

ley, 2003; Huerta and Rodgers, 2006; Lock and Willett, 2008). Adjacent sedimentation in the foreland imparts a downward advection of the isotherms due to the deposition of sediments at surface temperatures that are then buried (Husson and Moretti, 2002; Ehlers and Farley, 2003; Ehlers, 2005; Rak, 2015). Additional modifications to the thermal field arise from lateral heat flow across faults from emplacement of a warm hanging wall over a cool footwall, potential frictional heating on faults, and thickening of radiogenic heat-producing rocks (Brewer, 1981; Shi and Wang, 1987; Ruppel and Hodges, 1994; Ehlers and Farley, 2003). Taken together, these processes result in a crustal thermal field that is both temporally and spatially variable (Fig. 2).

Fold-and-thrust belts provide settings rich with geologic, geochemical, and geophysical signals of their thermal evolution. Examples of observations that provide insight into the thermal evolution of fold-and-thrust belts include: (1) quartz deformation temperatures (Grujic et al., 1996; Law et al., 2004, 2013; Long et al., 2011a; Law, 2014), (2) Raman spectroscopy of carbonaceous materials (RSCM) and vitrinite reflectance (Castaño and Sparks, 1974; Barker, 1988; Beyssac et al., 2004; Ruppert et al., 2010; Whynot et al., 2010; Cooper et al., 2013), (3) surface heat-flow determinations (e.g., Henry and Pollack, 1988), and (4) thermochronometry from a suite of different mineral systems, including, but not limited to,  $^{40}\text{Ar}/^{39}\text{Ar}$  of feldspar and mica, apatite and zircon fission-track dating, (U-Th)/He of zircon, apatite, and other mineral systems (e.g., Reiners and Ehlers, 2005; Table 1), and monazite geochronology (Robinson et al., 2003; Kohn et al., 2004; Kohn, 2008). Both quartz deformation temperatures and

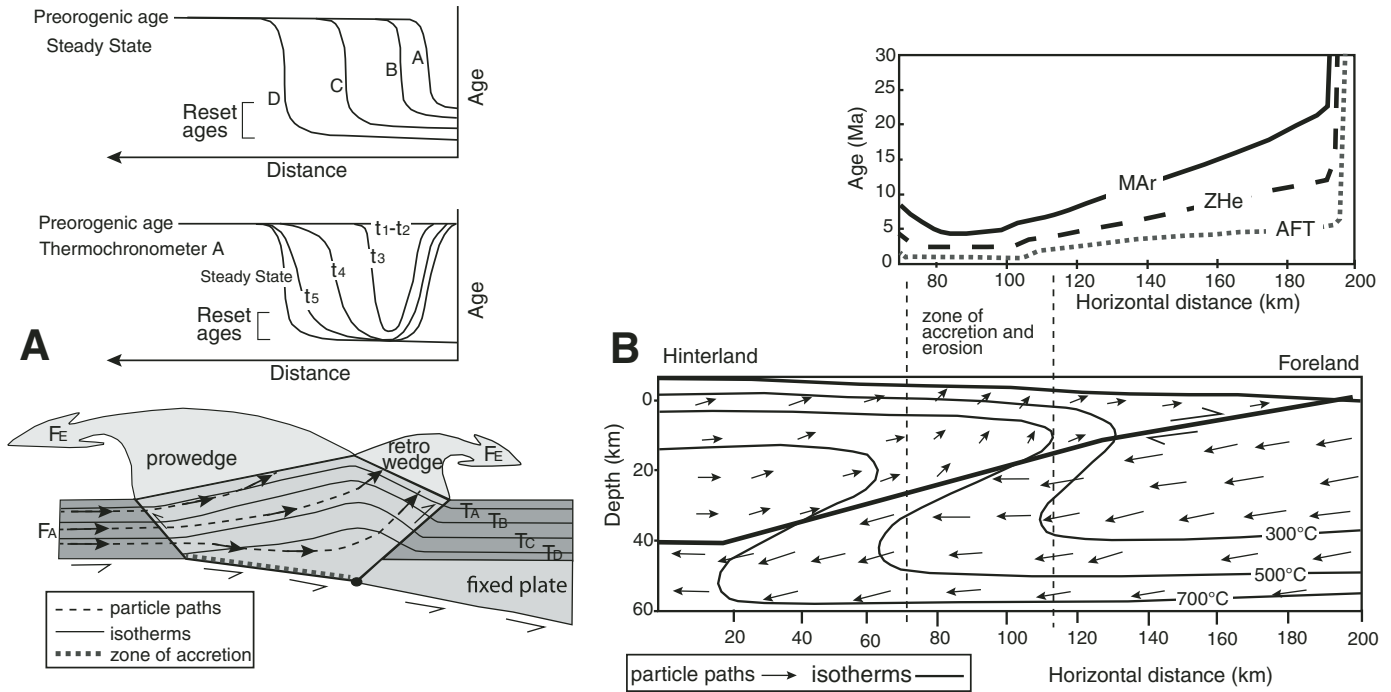


Figure 2. (A) Kinematic model for a critical wedge convergent orogen created by subduction and accretion (modified from Willett and Brandon, 2002). Top panel shows pattern of predicted ages from multiple thermochronometers (collected at the surface) at exhumational steady state. The zones of reset ages of four chronometers are nested and are concentrated along the retro wedge side of the model. Middle panel shows evolution with time ( $t$ ) of a single thermochronometer (A). Bottom panel shows kinematic model of a critical wedge. Accretionary flux,  $F_A$ , and erosional flux,  $F_E$ , determine material transport (dashed lines), while the vertical component of the material flux and erosion determine location and magnitude of warped isotherms. (B) Top panel shows predicted thermochronological ages vs. horizontal distance for a thermokinematic model of deformation in the central Nepal Himalaya (modified from Herman et al., 2010). Lines represent predicted ages for a thermochronometer: solid black line is  $^{40}\text{Ar}/^{39}\text{Ar}$  muscovite (MAr), long dash line is (U-Th)/He in zircon (ZHe), and gray dotted line is apatite fission-track (AFT). Dashed lines bracket region of accretion (duplexing) and erosion. Bottom panel depicts the thermal structure output from the numerical model (thin lines) and associated velocity field (small black arrows). Underplating/accretion zone matches with the high rock uplift zone.

RSCM provide insight into temperatures of the last deformation event or peak temperatures (respectively), while the other systems provide information on the temperature history and timing of exhumation or burial.

Observations of fold-and-thrust belt thermal evolution are commonly used to interpret the timing of events such as the age of maximum rock burial, or age of rock cooling due to exhumation. However, the ages of rock burial and exhumation can also be used to calculate thrust belt kinematics (e.g., displacement, velocity, acceleration/deceleration) when they are combined with both estimates of structural geometry as well as information about the subsurface thermal field from a thermal model. Models used to evaluate thermal observations range from simple simulations of a single fault, which numerically evaluate the effects of basal heat flow, radiogenic heat generation, and shear heating (e.g., Molnar and England, 1990; Royden, 1993; Henry et al., 1997), to single fault models that take into account both frontal accretion of material (the transfer of material from below to above the fault at the front of the system) and underplating (the transfer of material from below the fault to above the fault toward the hinterland of the system; e.g., Willett et al., 2001; Bollinger et

al., 2006; Herman et al., 2010). Numerical models used to predict thermochronologic data based on the geometry of a fault system include models that evaluate a single fault (e.g., Rahn and Grasmann, 1999; Huerta and Rodgers, 2006); a series of faults and fault geometries (e.g., ter Voorde et al., 2004; Lock and Willett, 2008); a simplified critical wedge system (e.g., Willett and Brandon, 2002; Bollinger et al., 2006; Herman et al., 2010); and the integrated signal from fault and fold geometries across an entire fold-and-thrust belt (McQuarrie and Ehlers, 2015).

Over the past few decades, technical advances in thermochronometry and thermokinematic numerical modeling have opened up an enormous opportunity to quantify the rates, magnitudes, and timing of deformation and erosion in active contractional settings. As a result, recognition has emerged that interpretations of thermochronometer data in compressional systems are linked to (1) transport of rocks along faults, (2) the location and magnitude of erosional exhumation, and (3) the mechanisms by which rock transport and erosion modulate the subsurface thermal field. Thus, accurate use of thermochronometer systems to place age constraints on fold-and-thrust belt kinematics requires understanding how the geometry and magnitude of fault slip

TABLE 1. ESTIMATED CLOSURE TEMPERATURES FOR COMMONLY USED THERMOCHRONOMETERS

Method	Mineral	Closure temperature* (°C)	Commonly used abbreviation	References
<sup>40</sup> Ar/ <sup>39</sup> Ar	Hornblende	400–600	HAr	Harrison (1982); Dahl (1996)
	Biotite	350–400	BAr	Grove and Harrison (1996); Harrison et al. (1985)
	Muscovite	300–350	MAr	Robbins (1972); Hames and Bowring (1994)
	K-feldspar	150–350	K-fels	Foland (1994); Lovera et al. (1991, 1997)
(U-Th)/He	Titanite	160–220	THe	Reiners and Farley (1999)
	Zircon	160–200	ZHe	Reiners et al. (2004)
	Apatite	55–80	AHe	Farley (2000)
Fission track	Titanite	240–300	TFT	Coyle and Wagner (1998)
	Titanite	380–420	TFT	Watt and Durrani (1985); Naeser and Faul (1969)
	Zircon (zero-damage)	330–350	ZFT	Tagami et al. (1998); Rahn et al. (2004)
	Zircon (“natural”)	230	ZFT	Brandon and Vance (1992); Brandon et al. (1998)
	Apatite	90–120	AFT	Laslett et al. (1987); Ketcham et al. (1999)

\*Closure temperatures calculated using Dodson (1973) for all systems except fission track. Dodson (1979) was used for the fission-track method using the 50% annealing isopleth (fanning) model. Closure temperatures provided are for a typical range of grain sizes and cooling rates between 1–100 °C/m.y.

Note: Table was condensed from that of Reiners (2005). See also Brandon et al. (1998), Hodges (2003), and Ehlers (2005) for additional information.

influence the distribution and amount of erosion and the resulting thermal structure of the crust. The purpose of this contribution is to review how both structures and the thermal field evolve in thrust belts and how linking these components together increases our ability to understand the temporal evolution of fold-and-thrust belt systems. We do this by structuring our discussion around (1) the mechanics and structure of thrust belts, which influence their thermal evolution; (2) the role of surface processes such as erosion and sedimentation on the thermal field; and (3) the ways in which the previously discussed tectonic and surface processes when combined together influence the composite thermal evolution of the thrust belt.

### Fold-and-Thrust Belts as Coulomb Wedges

The orogen-scale geometry of fold-and-thrust belts and accretionary prisms is wedge shaped, where the lower boundary is the basal detachment or décollement of the system, which slopes away from the tip of the wedge, and the upper boundary of the wedge is the topographic surface, which generally increases in elevation away from the tip of the wedge (e.g., Dahlen, 1990; Fig. 1A). Deformation within the wedge is dominated by thrust faults, which verge toward the wedge tip. The large-scale orogen geometry, pattern of deformation, associated exhumation, and state of stress can be approximated by critical wedge models (e.g., Chapple, 1978; Davis et al., 1983; Dahlen et al., 1984). The growth of the wedge is governed by conservation of mass. A critical taper ( $\theta_c$ ) equals the slope of topography ( $\alpha$ ) plus the slope of the décollement ( $\beta$ ) (Fig. 1A). Because of the requirement of mass conservation,  $\theta_c$  is simply a function of the strength of the material involved (assumed to be unvarying and nonco-

hesive) and the resistance to sliding imparted by basal friction. Thus, as more material is added to the system, both the width and the height of the wedge grow self similarly (Dahlen, 1990). This relationship requires that changes to this self-similar growth are the consequences of changes in the strength of the décollement, the strength of the material in the wedge, and/or preferential removal of material from the surface of the wedge (i.e., erosional control on topography; Dahlen, 1990).

Several variables have been shown to affect the behavior of Coulomb wedges. Wedges composed of strong rocks require a lower critical taper angle to propagate forward compared to wedges made up of weak rocks. Similarly, the presence of a weak basal layer reduces the critical taper angle required for the wedge to propagate forward (Davis and Engelder, 1985; Liu et al., 1992; Costa and Vendeville, 2002; Suppe, 2007; Malavielle, 2011). Theoretical and analogue models of critically tapered wedges provide a valuable conceptual framework for interpreting the first-order behavior of fold-and-thrust belts. An important contribution is that the balance between accretionary (material incorporated into the wedge) and erosional (material removed) fluxes determines whether an orogenic wedge grows, shrinks, or stays constant. If  $\theta < \theta_c$ , the rear of the wedge must shorten and thicken to increase  $\theta$  to a critical value. If  $\theta > \theta_c$ , the wedge may propagate outward to reduce  $\theta$  or lower the rear through normal faulting to reduce  $\theta$  (Fig. 1C). Thus, focused erosion in the hinterland of a system would promote out-of-sequence faulting there or enhance underplating (duplexing of strata) to regain critical taper (e.g., Malavielle, 2011). Numerical models emphasize this strong interdependence of deformation and erosion. Large-scale removal of mass causes the particle paths within the wedge to adjust to replace the eroded material (Willett et al., 1993).

Convergent orogens can have a strong feedback between the high rates of rock uplift and erosion (Willett and Brandon, 2002). Numerical models of convergent wedges evaluate how convergence, uplift, and erosion are coupled and how these coupled processes modify the subsurface thermal field (e.g., Willett, 1999; Willett et al., 2001). Topographic steady state is achieved when the average cross-sectional form of the topography, such as the mean elevation, the height of the main topographic divide, and the distance of the topographic divide from the deformation front, reaches a steady value (Willett and Brandon, 2002). In orogenic belts where erosion is high, it is possible for the system to reach an exhumational steady state where the erosional flux out of the system balances the accretionary flux into the system. This scenario is independent of a topographic steady state and will commonly postdate it in time (e.g., Willett, 1999). The subsurface temperature field of an orogen changes as a result of both the internal velocity field and the location of erosion (Fig. 2A). When numerically modeling convergent deformation at an orogen scale, Willett et al. (1993) showed that two critical wedges develop: a prowedge with the geometry and stress state of a critical wedge corresponding to a minimum taper angle, and a retrowedge, with the geometry and stress state corresponding to the maximum critical taper angle. When surface processes are added to the simulation, exhumation is most rapid and focused on the retrowedge side of the doubly verging simulation. While evaluating the response of orogens to changes in climate, erosion rate, tectonics, and rock uplift rate without requiring steady state, Whipple and Meade (2006) showed a strong climatic control on wedge width and diagnostic responses due to climatic or tectonic perturbations. Although the model relaxed the steady-state assumption, they did assume self-similar wedge growth and decay ( $\theta_c$  is constant) as modeled in sand-box experiments and numerical simulations (Davis et al., 1983; Koons, 1990; Hoth et al., 2006; Stolar et al., 2006). However, studies that use critical taper as a lens through which to interpret the kinematic behavior of a fold-and-thrust belt (Liu et al., 1992; DeCelles and Mitra, 1995; Horton 1999; Costa and Vendeville, 2002) emphasize the numerous and unexceptional processes that govern wedge evolution and force taper angle changes as the system evolves (i.e.,  $\theta_c$  is not constant; Fig. 1C).

Although critical wedge theory provides an important framework for understanding how orogen deformation responds to changing boundary conditions, the requirement that all rocks within the wedge are on the verge of Coulomb failure (Dahlen, 1990) and the inability to vary material properties within the wedge inhibit it from providing insight into the sequence of deformation that governs how a critical wedge develops from preexisting noncritical geometries. As pointed out by Stockmal et al. (2007), critical wedge solutions become more limited when evaluating the effect of material differences, particularly ones with original horizontal geometries, and the ways in which those initial planes of weakness impact the internal structural geometry, strain history patterns, and pressure-temperature-time paths within fold-and-thrust belts. This nonuniform behavior alters the

predicted erosional response and modifies the resulting thermal field. In addition, as surface processes change the shape or size of the wedge via erosion, they also change the behavior of the wedge via sedimentation (Fuller et al., 2006a; Stockmal et al., 2007; Willett and Schlunegger, 2010; Wu and McClay, 2011). Flexural subsidence and foreland deposition can result in a local critical or supercritical wedge that bypasses the need for the internal deformation commonly required to achieve critical taper. This process lends itself to widely spaced thrust faults that carry piggyback synorogenic basins (Stockmal et al., 2007; Wu and McClay, 2011).

## FOLD-AND-THRUST BELT STRUCTURES

### Original Basin Architecture

The critical wedge geometry of fold-and-thrust belts develops from a sedimentary prism that also has an initial wedge shape (Fig. 1B; Bally et al., 1966; Price, 1973; Chapple, 1978). Studies of North American fold-and-thrust belts have long recognized the association between patterns of deformation (particularly the location of thrust belt salients and recesses) and the location of Proterozoic and Paleozoic sedimentary basins (e.g., Thomas, 1977; Beutner, 1977; Hatcher, 1989; Boyer, 1995; Mitra, 1997). These observations emphasize the link between the inherited basin structure of passive margins and the development and evolution of large-scale structures that later deform these basins (Fig. 1A). Variations in the initial sedimentary basin taper and geometry (locations of mechanically strong and weak horizons) impart variations on the resulting fold-and-thrust belt geometry (Mitra, 1997; Boyer, 1995). For example, if the sedimentary prism has a low initial taper, high internal shortening is required for the wedge to advance. However, if the sedimentary prism has a high initial taper, the sedimentary prism may be stripped from the basement and advance as a single thrust sheet without undergoing significant internal shortening (Boyer, 1995; Mitra, 1997).

### Hinterland Megathrusts

The weak, low-initial-taper, distal portions of a passive-margin wedge will tend to have high internal strain and closely spaced structures in order to build critical taper and propagate forward. In contrast, the internal portions of a passive-margin sequence are regions that exhibit higher initial-taper angles and thick sections of stronger metasedimentary rocks that detach on weak sedimentary horizons, or brittle-ductile transition zones, to create hinterland megathrust sheets (Boyer and Elliott, 1982; Boyer, 1995; Mitra, 1997; Fig. 1). Megathrust sheets are remarkable for their length, thickness, and lack of internal deformation associated with transport (Hatcher and Hooper, 1992). They are common in the medial to hinterland parts of orogenic wedges. Examples include the Blue Ridge thrust sheet in the Appalachians (Boyer and Elliott, 1982; Hatcher and Hooper, 1992), the Canyon Range, Williard, and Lewis thrust sheets in the North

American Cordillera (Yonkee, 1992; van der Velden and Cook, 1994; DeCelles et al., 1995; DeCelles and Coogan, 2006; Hatcher, 2004), the Main Central thrust in the Himalayas (Schelling, 1992; Robinson et al., 2006; Long et al., 2011b), and basement megathrusts in the Bolivian Andes (Kley, 1996; McQuarrie and DeCelles, 2001; McQuarrie, 2002a). These megathrust sheets are generally 8–15 km thick and accommodate 100–350 km of displacement. If the thrust sheet detaches on the brittle-ductile transition zone, the basal detachment angle may stay close to  $0^\circ$  over a large area, creating a uniform slab geometry (Hatcher and Hooper, 1992; Hatcher, 2004). Duplexes and ramps form at the base of the megathrust sheets when the thrust fault can no longer propagate along the brittle-ductile transition zone (Fig. 1). These allow the megathrust to cut upward into the upper crust or sequence of platform sediments (Boyer and Elliott, 1982; Hatcher and Hooper, 1992) and transfer slip into the sedimentary sections in the front of the system (Mitra, 1997). The initial emplacement of megathrust sheets enhances the taper of the wedge by both elevating topography and increasing the décollement dip through isostatic loading (Stockmal et al., 2007; McQuarrie and Ehlers, 2015; Rak, 2015).

### Fault Bend Folds, Duplexes, and Imbricate Fans

Many of the map-scale folds that form in fold-and-thrust belts are the result of bending of stratigraphic layers over fault ramps (e.g., Rich, 1934; Rodgers, 1950; Gwinn, 1970; Suppe, 1983). Thrust faults tend to travel parallel to bedding along weak detachment horizons and step upward via fault ramps through strong layers into a higher bedding-parallel detachment layer (Rich, 1934). These fault bend folds tend to preserve layer thickness, and they produce no net distortion when the layers are hori-

zontal and conserve bedding dip (Suppe, 1983; Fig. 3A). The footwall ramps of these faults can range in height from less than 1 km to 10 km, increase structural elevation by bringing deeper rocks above their regional (stratigraphic) position, and impart an upward, vertical velocity to the motion of material. When multiple faults cut and repeat the same stratigraphic layer, an imbricate fan develops (Boyer and Elliott, 1982; Fig. 3B). If the thrust faults are spaced far enough apart, and fault slip is less than the fault spacing, the next fault to form does not alter the geometry or vertical motion of the fault preceding it; however, when faults are closely spaced and/or the slip on the fault is greater than the fault spacing, the motion of the next fault over the footwall ramp rotates previously formed thrust faults and ramps to steeper dips. When ramps sequentially develop between a lower and upper detachment surface, a duplex forms (Boyer and Elliott, 1982; Mitra, 1986). Each fault slice or volume of rock completely surrounded by faults (the top and bottom by décollement surfaces and each side by fault ramps) is called a horse (Boyer and Elliott, 1982; Fig. 3C). The geometry of a duplex is governed by the relationship between the length of each horse (or spacing between ramps) and the amount of displacement. If the length of the horse is greater than the amount of displacement, a hinterland-dipping duplex forms (Fig. 3C). If the amount of displacement is greater than the length of the horse, a foreland-dipping duplex forms (Fig. 3E). If the length of the horse is equal to the amount of displacement, an antiformal stack forms (Fig. 3D).

Thrusts generally develop in a forward-breaking sequence, defining a regional foreland-directed tectonic transport direction. Although the forelandward transport direction prevails, in detail, faults may move “out of sequence,” with reactivated or new fault motion anywhere in the hinterland of the frontal fault.

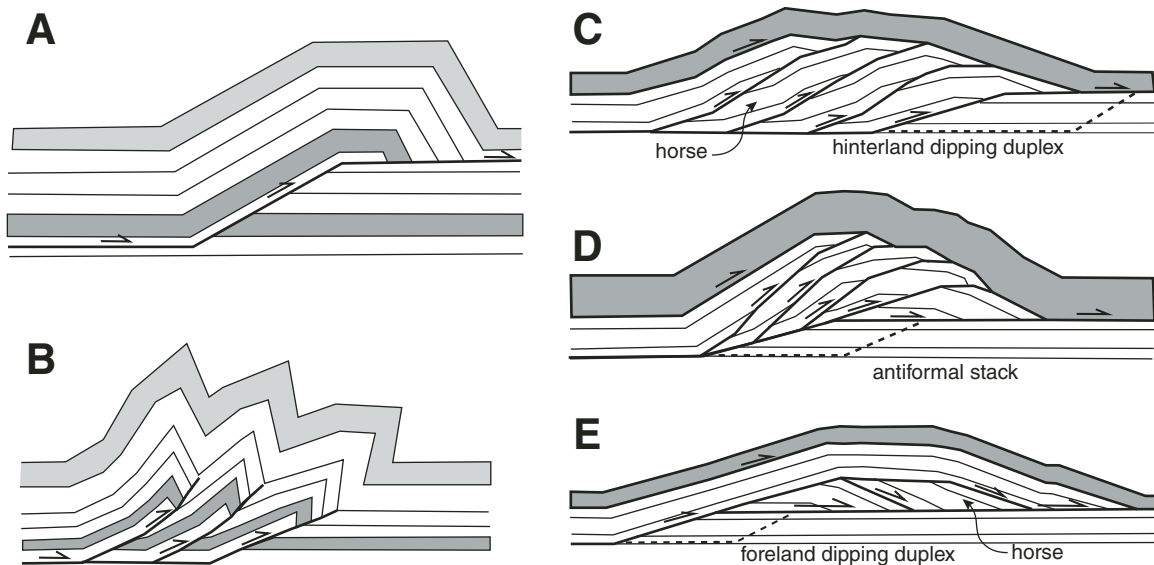


Figure 3. Typical fold-and-thrust belt structures (modified from McClay, 1992): (A) fault bend fold, (B) fault propagation fold/imbricate fan, (C) hinterland-dipping duplex, (D) antiformal stack, and (E) foreland-dipping duplex. Dashed lines represent location of the next fault to form.

As thrusting becomes closely spaced, out-of-sequence thrusting is inhibited as early thrusts steepen due to rotation of older thrusts by foreland thrust imbricates (Boyer and Elliott, 1982; Shaw et al., 2005). Tilting and folding of the earliest thrusts and the stratigraphy they carry make continued slip on them increasingly difficult. Any out-of-sequence faulting in the hinterland must cut across the original mechanical anisotropy of weak bedding horizons and faults. Because of this, maintaining a critically tapered wedge through continued uplift of the hinterland is generally facilitated by subsurface duplex growth (e.g., Malavielle, 2011).

### Foreland Uplifts

Thick-skinned, basement-involved thrust faults that extend into the midcrust (10–25 km) may be present in front of, and/or adjacent to, the frontal portions of fold-and-thrust belts (Smithson et al., 1978; Stone, 1993). These basement-involved structures are relatively broad, are short, often have variable strike directions and form irregular, anastomosing map patterns (Jordan and Allmendinger, 1986; Brown, 1988; Erslev, 1993; Kley et al., 1999). The uplifts are bounded by moderate to steep thrust faults that may include reactivated faults or inherited basement fabrics (e.g., Schmidt et al., 1993). The percent of shortening in these regions of basement faulting is notably less than in adjacent fold-and-thrust belts and typically ranges from 10% to 35% (Kley et al., 1999). Although preexisting structures such as reactivated normal faults (e.g., Kley et al., 1999; Pearson et al., 2013) are common in regions of foreland basement uplift, a more ubiquitous characteristic of these basement structures is the limited amount (2–5 km) of sedimentary rock overlying them (Brown, 1988; Erslev, 1993; Allmendinger and Gubbels, 1996; Allmendinger et al., 1997; Kley et al., 1999; McQuarrie, 2002b; Pearson et al., 2013). The deeper connection of these basement uplifts to the adjacent fold-and-thrust belts is still debated (e.g., DeCelles et al., 2004). However, if these intraforeland basement faults branch upward from a regional mid- or lower-crustal shear zone (Erslev, 1993; Pearson et al., 2013), then foreland basement uplifts may be integrated with the orogenic wedge (Livaccari, 1991; Erslev, 1993, 2001; Pearson et al., 2013; Reiners et al., 2015), and the different deformation styles simply reflect the deformational response of varying lithology and mechanical weaknesses.

### Foreland Basin System

Foreland basins are elongate sedimentary troughs formed between a fold-and-thrust belt and an undeformed craton (Price, 1973; Dickinson, 1974; Beaumont, 1981; Jordan, 1981; DeCelles and Giles, 1996). The basin is a function of the flexural distribution of a topographic load by the thrust belt on a viscoelastic plate (Beaumont, 1978, 1981; Jordan, 1981). The primary basin features formed due to this flexural response are a deep flexural trough (the foredeep depozone, ~2–6 km deep), the forebulge (a region of erosion or condensed sedimentation), and a zone of very minor (tens of meters for typical flexural rigidities) flexural

subsidence in the back-bulge region (e.g., DeCelles and Giles, 1996). A high magnitude of flexural subsidence may be focused in the frontal part of the orogenic wedge, producing accommodation for a zone of wedge-top sediment accumulation (Fig. 1).

### Accretionary Prisms

The study of accretionary wedges played a key role in the development of the critical wedge theory (Davis et al., 1983; Dahlen et al., 1984), and accretionary wedges have many similarities to fold-and-thrust belts exposed on land, including the characteristic wedge shape between the overlying topography and underlying basal décollement, a basal décollement that overrides undeformed rocks or sediments, and deformation that is dominated by imbricate thrust faults, duplexes, and related folds (Aoki et al., 1982; Behrmann et al., 1988; Moore et al., 1988; Dahlen, 1990; von Huene and Scholl, 1991; Adam et al., 2004; Smith et al., 2012). Significant differences between accretionary prisms and fold-and-thrust belts include the thickness of rocks incorporated into the growing belt, 7–15 km for fold-and-thrust belts and 0.2 km to 7.5 km for accretionary prisms (Price, 1973; Zhao et al., 1986; Hatcher, 1989; Roeder and Chamberlain, 1995; Mitra, 1997; Bernstein-Taylor et al., 1992; Smith et al., 2012); incorporation of unconsolidated sediments into accretionary wedges and the resulting arcward reduction of porosity and tectonic strain; and the rheologically uniform properties of ocean-floor sediments that comprise accretionary prisms, as opposed to the variable properties for fold-and-thrust belts (Bray and Karig, 1988; Moore et al., 1988; von Huene and Scholl, 1991; Taira et al., 1992). The lack of rheological contrast between the different sedimentary beds and the generally weak, water-rich sediments in accretionary prisms lead to more mechanically viable out-of-sequence faulting to maintain taper, as well as pervasively disrupted structure and strata and the formation of mélanges (Cloos, 1982; McCarthy and Scholl, 1985; Moore et al., 1988). Another process unique to accretionary prisms is subduction erosion of the overlying plate due to a lack of incoming sediments and/or a rough oceanic plate due to volcanic seamounts, plateaus, and ridges (von Huene and Scholl, 1991; von Huene et al., 2004). Thinning of the upper plate via subduction erosion changes the dynamics of the deforming wedge and may lead to long-term margin subsidence over wide regions of the wedge. This subsidence will enhance forearc basin growth as sedimentation continues during periods of strong basal erosion (von Huene and Scholl, 1991; Vannucchi et al., 2016).

### Balanced Cross Sections

Balanced cross sections were developed as a tool to produce more accurate and thus more predictive geological cross sections in the frontal, nonmetamorphic portions of fold-and-thrust belts (Bally et al., 1966; Dahlstrom, 1969), as well as a means of identifying the structures mentioned in the sections on hinterland megathrusts and fault bend folds, duplexes, and

imbricate fans. The technique also allows for quantification of fault displacement and fold shortening through palinspastic restoration. The criteria for the validity of any balanced cross section are that it is admissible and viable (Dahlstrom, 1969; Elliott, 1983). Admissibility is defined as a match between the structures drawn on the section and the structures that can be seen in the region of interest (Dahlstrom, 1969; Elliott, 1983). A viable section is a section that can be restored to an undeformed state; e.g., the material in the cross section must equal that in the restored section. The viability of a cross section rests on the assumption that if we truly understand how structures form, then we should be able to (1) take them apart (Elliott, 1983; Woodward et al., 1989) and (2) incrementally restore them to re-create the balanced section (McQuarrie, 2002a; McQuarrie et al., 2008; Robinson, 2008). However, balanced cross sections are nonunique, opening the possibility that different geometries and kinematics may be able to satisfy the same set of observations. The most nonunique aspects of cross sections are: (1) the geometry of structures that is not seen at the surface, and (2) the sequence of thrust faulting.

## SURFACE PROCESSES IN FOLD-AND-THRUST BELTS

Unlike normal faults, which tectonically exhume footwall rocks, thrust faults promote an increase in the mean surface elevation, but by definition, they do not by themselves allow for exhumation (the motion of rocks toward Earth's surface). Surface processes via fluvial, hillslope, or glacial erosion are required for rock exhumation and the generation of the sediment that ultimately resides in a foreland basin. Thus, motion on contractional structures creates elevated topography, but the exhumation pathway and cooling history of rocks toward the surface depend on the timing, rate, and magnitude of erosion, as well as on the geometry of the subducting plate (e.g., Ehlers and Farley, 2003; Shi and Wang, 1987; Huerta and Rodgers, 2006; Rahn and Grasemann, 1999; Lock and Willett, 2008; Bendick and Ehlers, 2014). Although the background thermal state of the upper crust is controlled primarily by basal heat flow and by crustal thermal properties such as thermal conductivity and heat production, focused erosion significantly perturbs the subsurface thermal field (Stuwe et al., 1994; Mancktelow and Graseman, 1997; Braun, 2002; Willett and Brandon, 2002; Ehlers, 2005). Thus, consideration of the thermal evolution of fold-and-thrust belts requires knowledge of the timing, rates, and location of erosion. Furthermore, as discussed later herein, the way in which erosion is distributed in a thermal-kinematic and erosion model of a fold-and-thrust belt can be a first-order control on the thermal history of exhumed rocks and therefore also on the way the kinematic history is interpreted. Finally, as mentioned in the section on fold-and thrust belts as Coulomb wedges, focused erosion may also influence where deformation occurs via Coulomb wedge theory (Dahlen, 1990; Willett, 1999; Willett and Brandon, 2002; Malavielle, 2011).

Thus, relating thrust structures to an evolving thermal field requires some estimate of how and when material is eroded and buried. Recent observational studies using low-temperature thermochronology (e.g., Lease and Ehlers, 2013; Thiede and Ehlers, 2013), cosmogenic radionuclides (e.g., Safran et al., 2005; Insel et al., 2010; Wobus et al., 2005), and tectonic geomorphology (e.g., Jeffery et al., 2013; Whipple and Gasparini, 2014) have sought to decipher the role of tectonics versus climate as the cause for patterns of denudation in fold-and-thrust belts. Studies on the way that surface processes respond to changes in tectonics and climate are complicated by factors such as the dynamics of Coulomb wedge deformation and their relation to erosion (e.g., Whipple and Meade, 2004, 2006), flexural-isostatic compensation of denudation and sedimentation, and Cenozoic climate and vegetation changes during orogen and fold-and-thrust belt formation (e.g., Kutzbach et al., 1993; Ehlers and Poulsen, 2009; Jeffery et al., 2014). These factors are often difficult to quantify, and in the following, we highlight simplified approaches currently used to (at least partially) account for them.

## Isostatic Response to Erosion and Sedimentation

The dip of the most recent or active décollement (as illustrated in any balanced cross section, or seismic section across a fold-and-thrust belt) is a function of both the original sedimentary taper of the sedimentary basin (Fig. 1; Bally et al., 1966; Price, 1973; Boyer, 1995; Mitra, 1997) and the progressive load of the fold-and-thrust belt, which increases the dip of the décollement angle ( $\beta$ ) through time (Stockmal et al., 2007; McQuarrie and Ehlers, 2015). As a fold-and-thrust belt grows with time, thrust faults uplift and deform the surface of Earth, creating a load that is flexurally accommodated. The flexural accommodation of the adjacent lithosphere results in a foreland basin (e.g., Price, 1973; Jordan, 1981; Beaumont, 1981). The lateral distribution of flexural subsidence migrates and deepens as faults continue to form, the basal décollement angle increases, and material is eroded from the fold-and-thrust belt (Fig. 4). Although erosion has a large effect on the location of deformation in critical wedge models (Willett, 1999; Malavielle, 2011), erosion in numerical models of fold-and-thrust belt deformation imparts relatively minor changes in deformation. These changes are less propagation toward the foreland and larger displacement and more well-developed duplexes in the hinterland in models that incorporate erosion. However, the style of faulting and the spacing between faults are remarkably similar in models with and without erosion. In contrast, isostasy and sedimentation have a profound impact on the location, magnitude, and style of deformation (Stockmal et al., 2007). The addition of isostasy progressively increases the critical taper ( $\beta$ ) due to thrust loading. This increase in taper promotes propagation of the thrust front (to reduce taper), which results in longer thrust sheets. The influence of syndeformational deposition on the modeled structural style that develops is significant. As the foreland basin deepens and  $\beta$  increases, the deformation front propagates out

into the foreland to a distance of several times the thickness of the wedge. This pattern is repeated as the wedge evolves (Stockmal et al., 2007). Applying these results to kinematic models emphasizes that an evolving fold-and-thrust belt must take into account the isostatic loading of thrust faults, the isostatic unloading due to erosion, and the development and propagation of a foreland basin with time.

There are two typical approaches for creating models of sequential deformation through fold-and-thrust belts. One approach moves forward with time, starting with an undeformed section and sequentially moving each fault to re-create the balanced cross section (e.g., McQuarrie, 2002a; McQuarrie et al., 2008; Robinson, 2008; Webb, 2013). The alternative approach starts with a balanced section and sequentially removes fault displacements and folds (Mora et al., 2010; Sak et al., 2012; Erdős et al., 2014). Both approaches reconstruct the sequential magnitude of fault displacement and folding, accurately calculate amount of shortening, and assess the kinematic evolution of the fold-and-thrust belt. However, only the forward approach allows for estimates of isostatic loading from fault motion or isostatic unloading via erosion. Sequentially removing fault displacement keeps the restored angle  $\beta$  the same as the modern  $\beta$ . As a result, the latter approach overpredicts rock depth at any time before present. As an example of the potential error magnitude introduced by this approach, a balanced cross section with 300 km of shortening and a modern  $\beta$  of  $3^\circ$  would suggest that shallow-marine rocks exposed at the surface today were originally in a position that was as deep as 15 km below the surface. The depth to which rocks are sequentially restored has a significant impact on their thermal history. Erdős et al. (2014) noted that a cooler crustal thermal structure was needed to match the measured high-temperature cooling data in the Pyrenees. Alternatively, the model could be restoring the rocks to a position that is too deep (thus becoming too warm) because thrust-related isostasy was not taken into account. Mora et al. (2015) encountered the opposite problem, in their model of the Eastern Cordillera of Colombia, where they noted that the modeled time-temperature paths did not reach the temperatures (potentially depths) required by HeFTy modeling of zircon

fission-track (ZFT) ages, suggesting more burial was needed in the model, possibly during the formation of the overlying foreland basin. These examples highlight not only the importance of erosion from isostatic loading of a fold-and-thrust belt, but also the importance of the way in which isostatic compensation is accounted for in a model.

### Modeling Surface Processes in Fold-and-Thrust Belts

Because of the inherent link between erosion and cooling of rocks in compressional orogens, modeling the evolution of a fold-and-thrust belt and the resulting thermal field requires an estimation of topography with time. Since the paleotopography of a mountain belt is extremely difficult to determine (e.g., Olen et al., 2012), a common practice is to assume the topography is in steady state throughout the modeled time period (e.g., Coutand et al., 2014; Herman et al., 2010; Robert et al., 2011; Whipp et al., 2007). Alternatively, early estimates of topography may be assumed to be muted versions of the modern topography, with topography increasing in relief with time (e.g., Erdős et al., 2014), or erosion may be assumed to be completely efficient, such that all topography is removed instantaneously (Lock and Willett, 2008). In this section, we highlight different simplifying assumptions about the ways in which erosion and erosion rates may vary spatially and temporally across a fold-and-thrust belt. Each method of estimating topography increases in complexity and its ability to estimate the erosional history and resulting topographic evolution.

### Erode It Flat

One way to estimate the magnitude of erosion that accompanies thrust belt deformation is to assume that no topography is generated, and the uplifted rocks are eroded to sea level. In this scenario, erosion keeps pace with uplift, such that all surface uplift generated by a thrust structure is removed instantaneously. Therefore, erosion rates will be high over a structure while it is active and nonexistent when the structure is inactive. This end-member scenario is most appropriate for thrust belts in which structural relief is large compared to topographic relief and

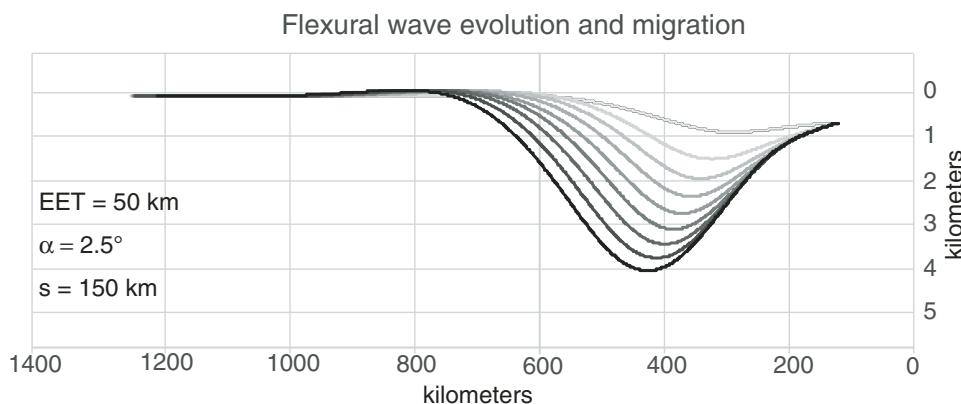


Figure 4. Generalized evolution and migration of foreland basin in 15 km increments. Total shortening ( $s$ ) is 150 km and is accomplished on two ramps (8 km high and 4 km high) spaced 30 km apart. For each 15 km increment of shortening, the fold-and-thrust belt propagates (i.e., ramps move forward) 30 km toward the foreland. The effective elastic thickness (EET) is 50 km, density is  $2700 \text{ kg/m}^3$ , and topographic slope ( $\alpha$ ) is  $2.5^\circ$ .

erosion occurs synchronous with fault motion, as has been suggested for Taiwan (Lock and Willett, 2008).

### **Erode to Taper**

Critical wedge theory argues that the upper topographic slope angle ( $\alpha$ ) remains constant if the strength of the deforming material, strength of the décollement, fluid pressures in the system, and slope ( $\beta$ ) of the décollement remain constant (Chapple, 1978; Davis et al., 1983; Dahlen, 1990). Thus, the topographic evolution of a fold-and-thrust belt through time can be estimated from the modern topographic slope. As a fold-and-thrust belt is reconstructed, this slope ( $\alpha$ ) would be applied over an initially narrow region of deformation, and as the fold and thrust belt grows and widens through time, the same  $\alpha$  would allow the fold-and-thrust belt to grow self similarly. As structures move and raise topography above the critical taper angle, erosion instantaneously lowers the surface back down to the taper angle (Robinson and McQuarrie, 2012). This critical taper angle model provides a slightly more “reality-based” approach to erosion than does the previous flat topography model.

Assuming a set critical taper or a flat topography creates an unsupported assumption that topographic elevations are not perturbed by isostatic loading. Thus, when isostasy is included in a kinematic model of deformation, isostasy will cause points in the model to subside, but topography will remain stationary (Gilmore, 2014). A constant angle slope also leads to a result that a natural topographic low between two structures may be artificially filled in to match the set critical angle. A solution to this is a modified critical taper angle, where elevated topography is generated using an assumed taper angle only where there is an increase in structural and surface elevation. At locations where new topography is not generated, the new topographic surface simply follows the old topographic surface. Thus, topography increases in elevation at the assigned angle everywhere structural elevation is increasing and stays the same or subsides where structural elevation is not generated. This approach allows topography to respond to deformational loading, erosional unloading, and sedimentation within fold-and-thrust belt systems (McQuarrie and Ehlers, 2015).

### **Surface Processes Modeling Approach**

Surface process models incorporate physics-based descriptions of surface erosion and sediment transport, which can include such processes as hillslope diffusion, fluvial incision, mass wasting, and glacial erosion into estimates of surface topography (Seidl and Dietrich, 1992; Chase, 1992; Beaumont et al., 1992; Seidl et al., 1994; Densmore et al., 1998; Willett, 1999; Whipple and Tucker, 1999; Yanites and Ehlers, 2012). Coupled one-dimensional (1-D) diffusion and fluvial incision models provide a significant, and physically based, improvement to predicting topographic evolution over active and inactive structures because they will approximate the valley and ridge topography seen in many fold-and-thrust belts (e.g., Appalachians, Taiwan, the Subandean portion of the Bolivian Andes). The shortcoming

of this approach is that it fails to describe the geometry of interfluves and distinguish between axial and transverse drainages, all of which may alter the near-surface thermal field.

Two-dimensional (2-D) planform surface process models predict the shape, size, and evolution of interfluves. Several modeling studies have investigated the sensitivity of low-temperature thermochronometers to topography with wavelengths and amplitudes comparable to interfluve geometries in active mountain belts (e.g., Stuwe et al., 1994; Mancktelow and Graseman, 1997; Braun, 2002, 2005). The conditions under which interfluve topography might influence the cooling rate of thermochronometer data and the closure temperature are entirely dependent on the exhumation rate, wavelength, and amplitude of the topography, as well as the temperature range of the specific thermochronologic system (Braun, 2002; Ehlers and Farley, 2003). Ehlers and Farley (2003) examined the effect of rugged (3.5 km relief) topography on subsurface isotherms and noted that with constant exhumation of 0.5 mm/yr, the apatite fission-track (AFT) closure depth was warped ~500 m over a 20 km distance. In a fold-and-thrust belt, this distance could encompass multiple structures that could alter age and modeled exhumation rate. Herman et al. (2010) evaluated the change in predicted thermochronometric ages between a critical slope topography that linearly decreased from 6 to 0 km across the Himalayan orogen and a 2-D planform surface model (CASCADE) that simulated an evolving river network with trunk streams and interfluves. The surface model predicted up to an ~2 m.y. variation in the predicted ages. The authors noted that although both models explain the general trends in the data, neither the original simplified kinematic model nor the linked kinematic and surface process model was able to reproduce the full variation in the data. Although topographic relief between interfluves may be important in some fold-and-thrust belts, we suggest that 1-D diffusion and fluvial incision models or the more simplified critical taper model that responds to regions of uplift or subsidence will account for the longest-wavelength, and most significant, topographic effect (i.e., valley and ridge topography) in the thermal calculation.

### **Sedimentation and Subsidence in Fold-and-Thrust Belts**

The frontal portions of many fold-and-thrust belts contain syndeformational piggyback basins and associated sedimentary strata that can be correlated to adjacent foreland basins (Ori and Friend, 1984; DeCelles, 1994; Pivnik and Johnson, 1995; Baby et al., 1995; Ramos et al., 2004). These basins highlight the interconnectedness among erosion, deformation, and sedimentation. If erosion keeps pace with deformation, then effective sediment transport will export large volumes of sediment into the foreland. Alternatively, if erosion cannot keep pace with growing structures, the structures have the potential to create sustained internal drainage conditions that trap sediment (e.g., Sobel and Strecker, 2003; Sobel et al., 2003; Hilley and Strecker, 2005) and reduce relief while potentially even increasing taper (Sobel et al., 2003; Fuller et al., 2006a; Willett and Schlunegger, 2010).

The influence of this syndeformational deposition on structural style and location may be profound. As the foreland basin deepens and the basal décollement  $\beta$  increases, the deformation front propagates out into the foreland to a distance of several times the thickness of the wedge (Stockmal et al., 2007). Continued sedimentation behind the thrust front increases taper and inhibits internal deformation in the piggyback basin (Fuller et al., 2006a; Stockmal et al., 2007; Willett and Schlunegger, 2010).

In addition to thrust loading and subsidence, in retroarc foreland basin systems, dynamic subsidence, related to viscous coupling of the mantle wedge, can increase the load experienced by the foreland and facilitate the increased preservation of foreland basin sedimentary rocks (DeCelles, 2012). The thickness and distribution of sedimentary basins in retroarc subduction zones commonly require an additional component of subsidence to account for the depth and location of foreland basin deposits (Mitrovica et al., 1989; Gurnis, 1993; Catuneanu, 2004; DeCelles, 2012). Sedimentary strata preserved in the North American Cordillera strongly suggest a component of dynamic subsidence in addition to flexural subsidence related to thrust-fault loading (Gurnis, 1992, 1993; Painter et al., 2014). Dynamic subsidence has also been proposed to account for the modern magnitude and distribution of foreland basin sedimentary strata in the Central Andes (Horton and DeCelles, 1997).

## THERMAL STRUCTURE OF FOLD-AND-THRUST BELTS

The background thermal state of continental crust is primarily controlled by the flux of heat at the base of the crust, the surface temperature, radiogenic heat production within the crust, and thermal diffusivity (e.g., Chapman, 1986). Deviations from this background state can occur by a variety of processes. For example, magmatism can provide a temporary heat source at different depths within the crust, and near-surface and crust-scale fluid flow can both increase or decrease thermal gradients depending on the flow path (e.g., Ehlers and Chapman, 1999; Whipp and Ehlers, 2007). Erosion and sedimentation can increase or decrease, respectively, thermal gradients depending on the rate and duration of the event (e.g., Mancktelow and Graseman, 1997; Ehlers, 2005). Additional deviations can occur from topography that can locally increase or decrease upper-crustal thermal gradients beneath valleys and ridges, respectively (e.g., Lees, 1910; Lachenbruch, 1968; Braun, 2005). Furthermore, faulting can influence the crustal field through a variety of processes. First, at sufficiently high slip rates, shear heating can provide a local heat source along a fault plane (e.g., Molnar and England, 1990). Second, faulting can increase topographic relief, thereby enhancing erosion, and also creating accommodation space for sedimentation. Third, thrust faulting can result in crustal thickening and therefore an increase in the thickness of radiogenic heat-producing elements as a crustal heat source (e.g., Furlong and Edman, 1984, 1989). Previous reviews and in-depth discussions of these topics have been presented in the reviews of Hae-

nel et al. (1988), Furlong et al. (1991), Ehlers (2005), and Braun (2005). In the following, we discuss some of these processes and their interactions with the previously mentioned fold-and-thrust belt deformation processes, and the ways in which thermal and deformation processes together lead to spatial variations in the thermochronometer ages used to infer the kinematic history.

## Modification of Thermal Field in Critical Wedges

Early analytical and finite-element numerical models of thrust belts and accretionary prisms evaluated the effects of mantle heat flow, convergence rate, erosion rate, accretion rate, heat production, and fault friction on the thermal structure of simplified wedge-shaped thrust systems (Barr and Dahlen, 1989; England et al., 1992; Royden, 1993; Henry et al., 1997). Royden (1993) showed that at the toe of these wedge systems, where the distance between the fault and the erosion surface is thin (~5 km), high erosion, accretion, and heat production have almost no effect on the thermal structure. However, as this distance increases (20–30 km), erosion, accretion, and heat production exert a very large control on the thermal structure of the wedge. Significant outcomes of these early studies were that in the absence of erosion, the temperature of the upper plate remains cool, and the magnitude of erosion was shown to have the largest effect on the temperature structure of the upper plate (Royden, 1993; Henry et al., 1997). Henry et al. (1997) noted that while frictional heating produces heat flow of 24–47 mWm<sup>-2</sup> in the upper plate, shear stress drops quickly in the brittle-ductile transition zone, limiting heating at higher temperatures and larger depths in the crust. In models that include both erosion and accretion, it was assumed that erosion exactly balanced accretion and uplift (Royden, 1993; Henry et al., 1997; Avouac, 2003; Bollinger et al., 2006), so that the system remained in a flux steady state (Willett and Brandon, 2002).

In early models, the magnitude of accretion was constant across the entire fault length, while erosion was constant across the entire topographic surface (Royden, 1993; Henry et al., 1997). In later models, tuned to specific orogenic systems, a narrower window of accretion was specified, where continuous material transfer occurred across the fault from the lower plate to the upper plate (e.g., Bollinger et al., 2006; Herman et al., 2010). Topography was still assumed to be in steady state, and so the location of rock uplift over ramps and locations of focused accretion drove focused erosion in these regions. In turn, areas of high erosion resulted in compressed isotherms and high heat flow (Bollinger et al., 2006; Herman et al., 2010; Coutand et al., 2014; Fig. 2B).

The importance of erosion for the thermal structure of critical wedges was also explored in numerical models of doubly vergent wedges. Similar to other analytical and numerical models, the location of exhumation had the largest control on the resulting thermal field, because of the strong feedback between the location of rock uplift and erosion (Willett and Brandon, 2002; Fuller et al., 2006b). Similar to single fault models, areas of high

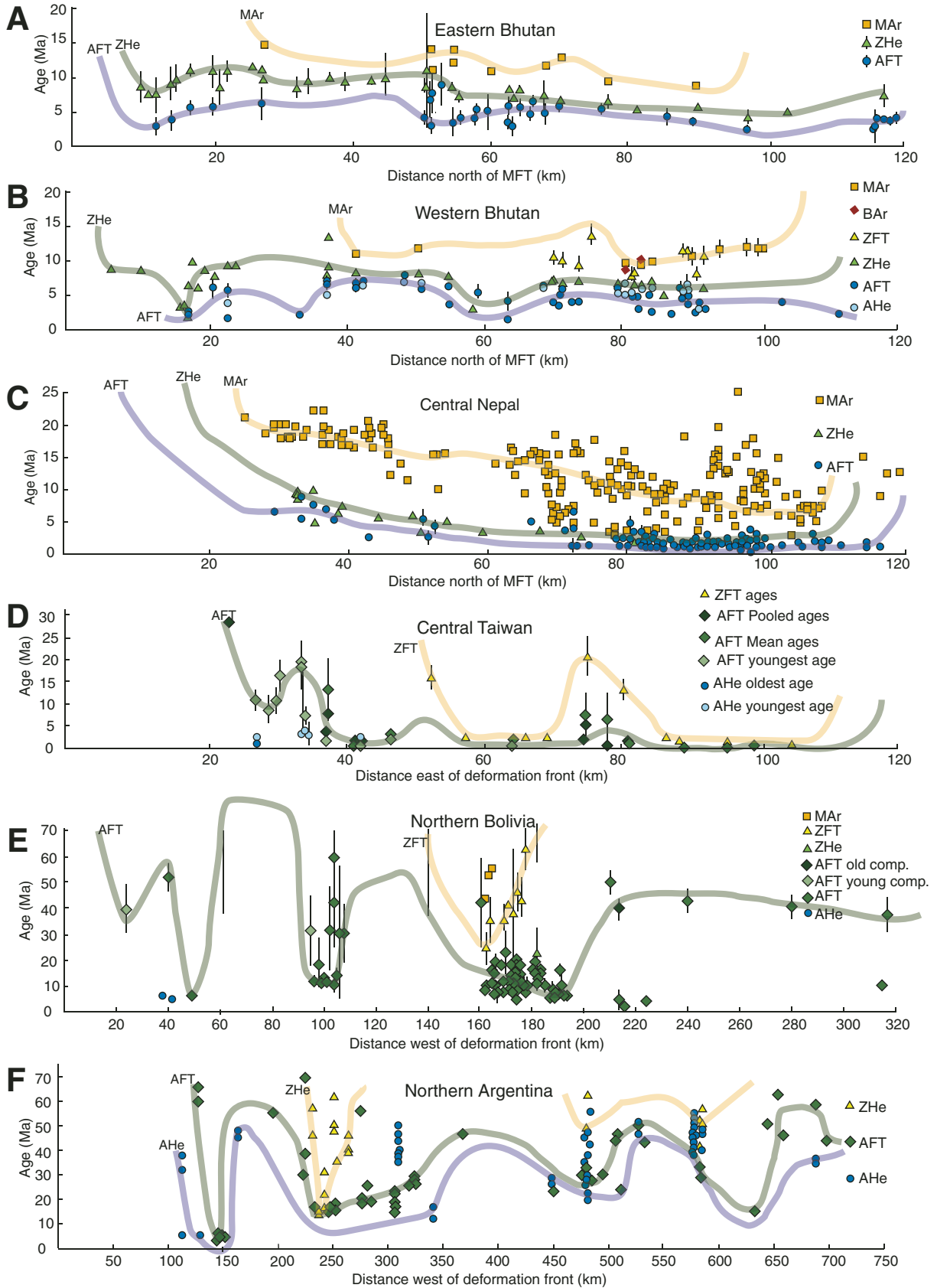


Figure 5.

erosion result in elevated, compressed isotherms near Earth's surface (Fuller et al., 2006b). In doubly verging critical taper simulations, rock uplift and the associated exhumation were most rapid and focused on the retrowedge side of the wedge (Willett, 1999; Fig. 2A).

### Thermal Structure and the Spatial Patterns of Cooling Ages

Recent advances in thermochronometry combined with the strong link between erosional exhumation and the resulting thermal field have promoted the use of thermochronometers (Table 1) as a key tool in documenting the thermal history of rocks and estimating their deformation and exhumation path (e.g., Reiners and Brandon, 2006; Huntington et al., 2007). A common approach in determining a geothermal gradient from a suite of thermochronologic samples, as well as ascertaining the magnitude of exhumation, is a vertical transect of ages, where at least two or three samples have ages that have been fully reset. The vertical profile provides bedrock cooling ages as a function of depth in an orogen. Although it is rarely possible to sample a truly vertical transect, mountainous regions often provide a close approximation to a true vertical sampling approach (Wagner and Reimer, 1972; Fitzgerald et al., 1995; Reiners et al., 2000; Stockli et al., 2000; Whipp et al., 2007; Fosdick et al., 2013). While vertical transects constrain temporal changes in exhumation rates at a given location, sampling over broad areas in an orogen provides insight into spatial patterns of exhumation magnitudes and rates (Fig. 5; e.g., Willett and Brandon, 2002; Reiners and Brandon, 2006). Spatial patterns of thermochronometric ages in convergent orogens have either been interpreted as a result of individual structures, such as motion on discrete faults or folds (Wobus et al., 2003; Pearson et al., 2013; Carrapa et al., 2011), or, more commonly, they have been interpreted with respect to the overall movement of material through an orogenic system (Batt et

al., 2001; Willett and Brandon, 2002; Fuller et al., 2006b; Huntington et al., 2007; Herman et al., 2010; Thomson et al., 2010; Reiners et al., 2015). In this context, the basal décollement, the rate of accretion from below the fault to above the fault, and the location where erosion is focused determine the particle paths and orogen-scale thermal structure (Fig. 2), but individual structures are considered ephemeral. As mentioned previously, the location of focused exhumation in these orogen-scale models elevates temperature isotherms and determines the location of the youngest and deepest reset thermochronometers (Willett and Brandon, 2002; Herman et al., 2010). For doubly vergent wedge systems such as that illustrated in Figure 2A, the prediction is that reset-age zones will be nested adjacent to the retrodeformation front where rock uplift has the strongest vertical component. The degree to which this nested pattern is developed is used as an important measure of the maturity of an orogenic system (Willett and Brandon, 2002; Fig. 2A). If only a portion of the orogenic system is being evaluated, many model frameworks require that the fault has a fixed location in the center of the model and may incorporate some component of frontal accretion or underplating by assigning a flux of material across the fault. The fixed reference frame model requires that convergence is partitioned into an overthrusting rate, which advects hot material toward an eroding surface, and an underthrusting rate, which advects cool material to deeper depths. As in entire orogen models, the youngest reset thermochronometers are in the region of high erosion. Assuming a steady-state topography, the region of high erosion is also the region of focused accretion, where material is transferred from the underthrusting plate to the overriding plate. If the rate of overthrusting is faster than the rate of accretion, the recently exhumed material is transferred toward the foreland, and thermochronometer ages gradually get older in that direction (Herman et al., 2010; Fig. 2B). The spatial distribution of orogen-scale thermochronologic ages (Fig. 5) provides support for both exhumation and cooling due to continuous particle path flow, as discussed in this section (Fig. 2), as well as support for exhumation focused over individual, discrete structures, which will be discussed in the following section (Fig. 6).

All fold-and-thrust belts and accretionary prisms are composed almost entirely of rocks that were scraped off of the lower plate (footwall of the system) and added to upper plate (hanging wall) of the system, indicating the importance of both accretion and erosion in the modern-day surface expression of these systems and their thermal history (Fig. 2). However, these models highlight the extreme sensitivity of the resulting thermal structure of the fold-and-thrust belt to the location of accretion and erosion, indicating that the thermal structure would be sensitive to the ways in which these locations may have evolved (moved) through time.

### Modification of the Thermal Field by Thrust Faults and Focused Erosion

While early analytical models highlighted the shallow portions of a thrust system (5–10 km deep) that produce only minor

Figure 5. Age vs. distance plots of thermochronologic data from the Himalaya, Taiwan, and the Andes (symbols). Transparent lines were manually drawn to highlight variations in the spatial trends of cooling ages that may be the result of the geometry and age of structures. MFT—Main Frontal thrust. (A)  $^{40}\text{Ar}/^{39}\text{Ar}$  muscovite (MAr), (U-Th)/He in zircon (ZHe), and apatite fission-track (AFT) ages for eastern Bhutan (91°E–91°30'E; data from Long et al., 2012; Coutand et al., 2014; Adams et al., 2013); (B) MAr,  $^{40}\text{Ar}/^{39}\text{Ar}$  of biotite (BAr), zircon fission-track (ZFT), ZHe, AFT, and apatite (U-Th)/He (AHe) ages for western Bhutan (89°30'E–90°E; data from McQuarrie et al., 2014; Coutand et al., 2014; Adams et al., 2015); (C) MAr, ZHe, and AFT ages for Central Nepal (84°E–85°30'E; data summarized in Herman et al., 2010; Cross, 2014; Khanal, 2014); (D) ZFT, AFT, and AHe ages for central Taiwan (24°N–24°30'N; data summarized in Fuller et al., 2006b; Lock, 2007); (E) MAr, ZFT, ZHe, AFT, and AHe ages for northern Bolivia (15°S–17°S; data from Benjamin et al., 1987; Barnes et al., 2006, 2012; Gillis et al., 2006; Safran et al., 2006; McQuarrie et al., 2008); and (F) ZHe, AFT, and AHe ages for northern Argentina (23°S–27°S; data summarized in Reiners et al., 2015). Deformation front indicates foreland limit of all deformation.

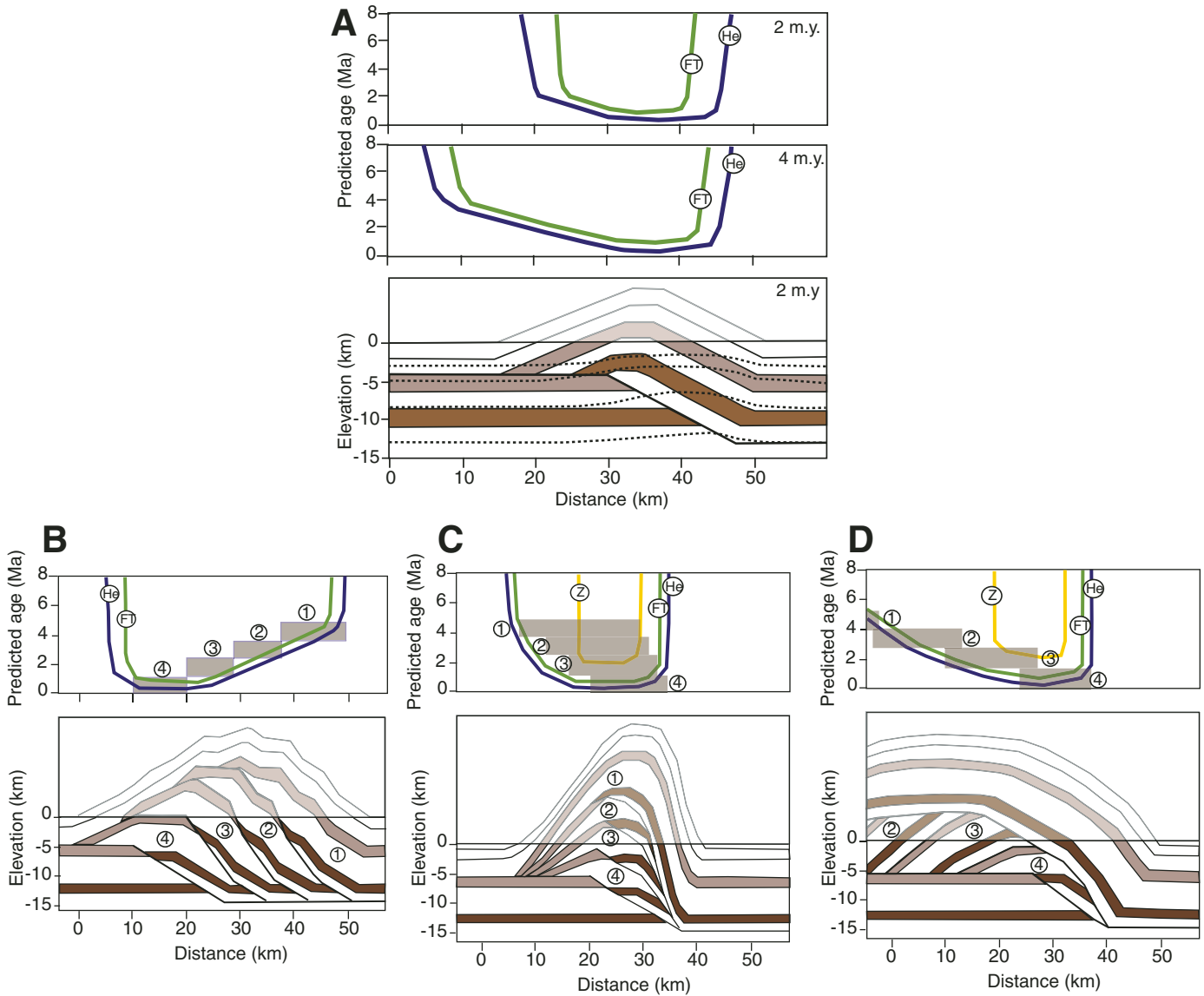


Figure 6. Patterns of thermochronometric age vs. distance generated during thrust faulting (modified from Lock and Willett, 2008). (A) Fault bend fold with resulting modification of thermal field and predicted pattern of apatite fission-track (FT) and apatite (U-Th)/He (He) ages after 2 m.y. (top panel) and 4 m.y. (middle panel) of deformation. Bottom panel shows resulting structure and location and amount of erosion. (B–D) Structure and resulting patterns of thermochronometric age vs. distance generated during formation of a hinterland-dipping duplex (B), antiformal stack (C), and foreland-dipping duplex (D). Numbers represent order of deformation, and gray bars represent area and age of uplift.

adjustments to the thermal field (Royden, 1993), individual structures can produce surface uplift over footwall ramps, and similar to orogen-scale models, the zone of rock uplift focuses erosion and exhumation. Series of studies have examined the modification of the subsurface thermal field by individual structures or sets of structures (ter Voorde et al., 2004; Huerta and Rodgers, 2006; Lock and Willett, 2008). These studies have shown that both surface uplift via faulting (ter Voorde et al., 2004; Huerta and Rodgers, 2006) and erosion focused over regions of active uplift (Huerta and Rodgers, 2006; Lock and

Willett, 2008) modify the subsurface thermal field (Fig. 6A). Motion of material over a thrust ramp raises isotherms upward, where the rock velocity has a vertical component, and depending on the magnitude of erosion, these isotherms become compressed (ter Voorde et al., 2004; Huerta and Rodgers, 2006; Lock and Willett, 2008). The location and magnitude of exhumation associated with motion over a ramp produce a characteristic “U-shaped” pattern of predicted exhumed cooling ages along a transect perpendicular to the thrust structures. The pattern is formed by the distribution of reset, partially reset, and unreset

cooling ages, with the youngest reset ages focused above the thrust ramp (Lock and Willett, 2008; McQuarrie and Ehlers, 2015). In the following, we use the terms reset, partially reset, and unreset as defined by Brandon et al. (1998). The key point for this study is that reset ages refer to ages that are younger than the depositional or intrusive age of the rocks from which they come and are interpreted to represent cooling associated with the most recent tectonic event.

### **Fault Bend Folds**

In a simple model with a single fault bend fold (Fig. 6A), the deepest material exhumed is located in the hanging wall directly above the ramp. Here, vertical motion of material and focused erosion of the hanging wall produce an upward deflection of isotherms and the first reset ages due to fault motion and subsequent exhumation (Lock and Willett, 2008). Consistently young ages are located above the thrust ramp and form the flat base of the “U-shaped” thermochronometric age pattern. As faulting continues to move material laterally along the upper flat, the initially reset ages become older with time due to no uplift and minimal exhumation, while the youngest ages continue to be focused over the active ramp. Thus, the oldest fully reset thermochronometer age (in the direction of transport) indicates when the faulting initiated, while the difference between the oldest and youngest reset ages indicates fault duration (Huerta and Rodgers, 2006; Lock and Willett, 2008; McQuarrie and Ehlers, 2015).

### **Imbricate Fans**

Imbricate fans are structures formed by series of faults that cut through the stratigraphy, each creating a fault ramp (Fig. 3B). When these structures are spaced far enough apart that the ramps do not interact with each other, the material in the hanging wall of one fault is not deformed by successive faults. The cooling age pattern associated with each thrust sheet records uplift and exhumation related to each individual structure and shows the same “U-shaped” thermochronometric age pattern as in the individual fault models (Lock and Willett, 2008). When the faults are more closely spaced (Fig. 3B), the geometry of the faults and their subsequent cooling patterns are no longer independent of each other. Inactive faults toward the hinterland are rotated, deformed, and exhumed as they experience upward motion along the ramp of an active fault in the foreland. The pattern of predicted ages becomes a single “U-shape” similar to rocks exhumed by an individual thrust (Lock and Willett, 2008). Closely spaced faults create a smooth age increase from the youngest reset ages focused over the most recent active fault to the oldest reset cooling ages over the first ramp in the system (Lock and Willett, 2008; Fig. 6B). The smooth pattern from the oldest reset age to the youngest reflects exhumation associated with slip on each subsequently younger fault and motion up each associated ramp. The modeled cooling pattern shows no distinct change or break in the thermochronometric age moving from the hanging wall to the footwall of a fault, even when the

thrust ramps are exhumed (Lock and Willett, 2008; McQuarrie and Ehlers, 2015).

### **Duplexes**

Like imbricate fans, duplex systems are composed of a stack of faults and their associated footwall ramps (Fig. 3). In a hinterland-dipping duplex, where each fault gets younger in the direction of transport, the cooling pattern produced is identical to a closely spaced imbricate fan, where reset cooling ages gradually get younger in the direction of transport, and the youngest cooling ages are focused over the active ramp (Fig. 6B). For a foreland-dipping duplex, the same relationship between age of faulting and location of youngest cooling ages holds true; however, because fault displacement is much greater than fault spacing, the youngest reset ages are concentrated above the active ramp, but the reset ages get systematically older in the direction of transport (Fig. 6D). This spatial pattern occurs because material is first exhumed above the active fault ramp and is then horizontally transported to a position beyond where the next ramp forms (Lock and Willett, 2008). With this geometry, the active ramp is always behind, or hinterlandward of the growing duplex, while the first horse (Figs. 3 and 6D), and the cooling signal associated with it, has been translated the most toward the foreland (e.g., Boyer and Elliott, 1982). For an antiformal stack, where the fault ramps are stacked on top of each other, a much more narrow U-shaped pattern is formed with a greater magnitude of exhumation and resetting of higher-temperature chronometers (Lock and Willett, 2008; Fig. 6C).

### **Modification of the Thermal Field by Flexure and Sedimentation**

Rapid sedimentation of cold, low-conductivity sediments depresses the isotherms in sedimentary basins (Carslaw and Jaeger, 1959; Lucazeau and Le Douran, 1985; Husson and Moretti, 2002). Modeling studies have shown that even moderate sedimentation rates (~0.2 mm/yr) lower the heat flow in sedimentary basins (Ehlers, 2005; Theissen and Rüpke, 2009). Fold-and-thrust belts and foreland basins have long been recognized as linked systems (e.g., Price, 1973; Dickinson, 1974; Beaumont, 1981; Jordan, 1981; Ori and Friend, 1984; Burbank et al., 1992; DeCelles, 1994; DeCelles and Mitra, 1995; Pivnik and Johnson, 1995), where a significant portion of the fold-and-thrust belt may have been buried by a migrating foreland basin (Royse, 1993; DeCelles and Mitra, 1995; DeCelles and Horton, 2003; Stockmal et al., 2007). Thus, at least a portion of the thermal history of a fold-and-thrust belt is inherently tied to the sedimentation history of the associated foreland basin.

Thermokinematic modeling, such as presented in the previous section, indicates different exhumation magnitudes are necessary to reset the same thermochronometer based on the location of the sample in the fold-and-thrust belt–foreland basin system. Rocks that were exhumed early in the deformational history require less exhumation (3–4 km of exhumation

to reset AFT ages) than rocks that were exhumed later in the history and were buried by an evolving foreland basin. Rocks buried in a foreland basin required over ~6 km of exhumation to reset AFT ages, because active sedimentation cools the geothermal gradient (Husson and Moretti, 2002; Ehlers, 2005; Rak, 2015). Thus, differences in required exhumation magnitude for the same thermochronometer are a result of the effects of erosion and sedimentation on the near-surface thermal field (Husson and Moretti, 2002; Rak, 2015). If the time period between foreland basin burial and subsequent exhumation is short, then more exhumation is required to reset low-temperature thermochronometers (because the geothermal gradient remains depressed). However, if the time window between deposition and exhumation is long, then the geothermal gradient has time to equilibrate or to keep pace with the sedimentation rate, facilitating a warmer gradient, and requires less exhumation to reset low-temperature chronometers (Rak, 2015).

### Material Properties—Effect of Heat Production on Predicted Cooling Ages

In addition to the modification of the thermal field by active faulting, erosion, and sedimentation, the thermal state of the crust depends on the basal heat flow from the mantle and the material properties of the crust (e.g., thermal conductivity, density, heat capacity, and radiogenic heat production). Radiogenic surface heat production can vary spatially by large amounts (e.g., Mareschal and Jaupart, 2013) and is a function of the concentration of heat-producing elements in the crust. Systematic sampling of crustal rocks now exposed at the surface indicates that heat production diminishes with depth through the crust and that this decline is not monotonic (Ketchum, 1996; Brady et al., 2006). Although both horizontal and vertical variability exists, the crustal geotherm is not sensitive to the exact vertical distribution of heat production and depends most strongly on the thickness of enriched upper-crustal rocks (Mareschal and Jaupart, 2013). Thus, multiple model combinations with different surface radiogenic heat production values, different depths to which high heat production tapers off to background values (e-fold depth), and different thermal conductivity and basal heat flux values may all produce similar crustal thermal structures.

In thermokinematic models, changing heat production values will change the predicted cooling ages (e.g., Whipp et al., 2007; McQuarrie and Ehlers, 2015; Gilmore, 2014; Rak, 2015). To a first order, a change in the surface radiogenic heat production values does not affect the across-strike pattern or shape of the cooling curve (Fig. 7) but rather imparts a vertical shift to the ages, where lower radiogenic heat production produces lower thermal gradients and older cooling ages (with all other factors being equal). However, altering the thermal history of the model by imparting a hotter or colder thermal field can also result in a different cooling pattern preserved at the topographic surface if the exhumation amount is close to a particular closure temperature for a thermochronometric system.

### Thrust Systems

In fold-and-thrust belt systems, all of the previously discussed structures may occur in any order and thus modify and reset the cooling age patterns imparted by the first series of structures to form. Each component in a fold-and-thrust belt system imparts a characteristic cooling pattern seen in the predicted ages at the surface. Rocks collected and measured at the surface record cooling associated with every stage of the structural evolution. However, the events that are recorded by any given thermochronometric system are dependent upon the magnitude of exhumation associated with each set of structures and the thermal history of the rocks influenced by the length and magnitude of burial, speed of exhumation, and heat production (Gilmore, 2014). To illustrate how previously set cooling patterns are modified by later structures, we present a sequentially deformed cross section and the associated predicted cooling ages across the Himalayan fold-and-thrust belt in Bhutan. The sequential model is modified from Gilmore (2014) and Long et al. (2012), and the cooling ages were modeled following the procedure outlined in McQuarrie and Ehlers (2015). In this modeling approach, a geologic cross section through a fold-and-thrust belt is sequentially deformed, taking into account flexural loading from thrusts and unloading due to erosion (Robinson and McQuarrie, 2012; McQuarrie and Ehlers, 2015) as discussed in the “Isostatic Response to Erosion and Sedimentation” section, with topography estimates as outlined in the “Erode to Taper” subsection of the “Modeling Surface Processes in Fold-and-Thrust Belts” section.

In this simulation, the first structure to form is the Main Central thrust (Gansser, 1964; LeFort, 1975; Hodges, 2000), which is emplaced over a footwall ramp and on top of lower Lesser Himalaya rocks (Long et al., 2012). After 50 km of shortening has accumulated, time slice A (Fig. 8) illustrates the general U-shaped pattern of cooling ages observed and predicted above a simple footwall ramp (Lock and Willett, 2008; Fig. 6A). Directly over the northern edge of the footwall ramp, the predicted zircon (U-Th)/He (ZHe) and AFT ages range from unreset to partially reset. The youngest reset ages occur at the upper limit of the footwall ramp and become systematically older in the displacement direction south (left) of the ramp until the southern edge of the Main Central thrust is reached. In time slice B (Fig. 8), the previous cooling pattern has been modified by the development of a southward-propagating duplex. The southward-younging age pattern seen in the predicted AFT and ZHe ages is youngest immediately above the active ramp. The exhumation associated with this duplex formation has allowed for reset  $^{40}\text{Ar}/^{39}\text{Ar}$  in muscovite (MAr); however, the pattern of the reset MAr ages reflects the northward-younging cooling associated with the earlier emplacement of the Main Central thrust in panel A (gray arrow, Fig. 8B). The next two pulses of cooling are initiated by motion of material over a footwall ramp, which causes a northward-younging pattern of cooling ages (Fig. 8C), and the development of the upper Lesser Himalaya duplex, which grows southward and initiates a southward-younging pattern in the predicted ZHe and AFT ages (Fig. 8D).

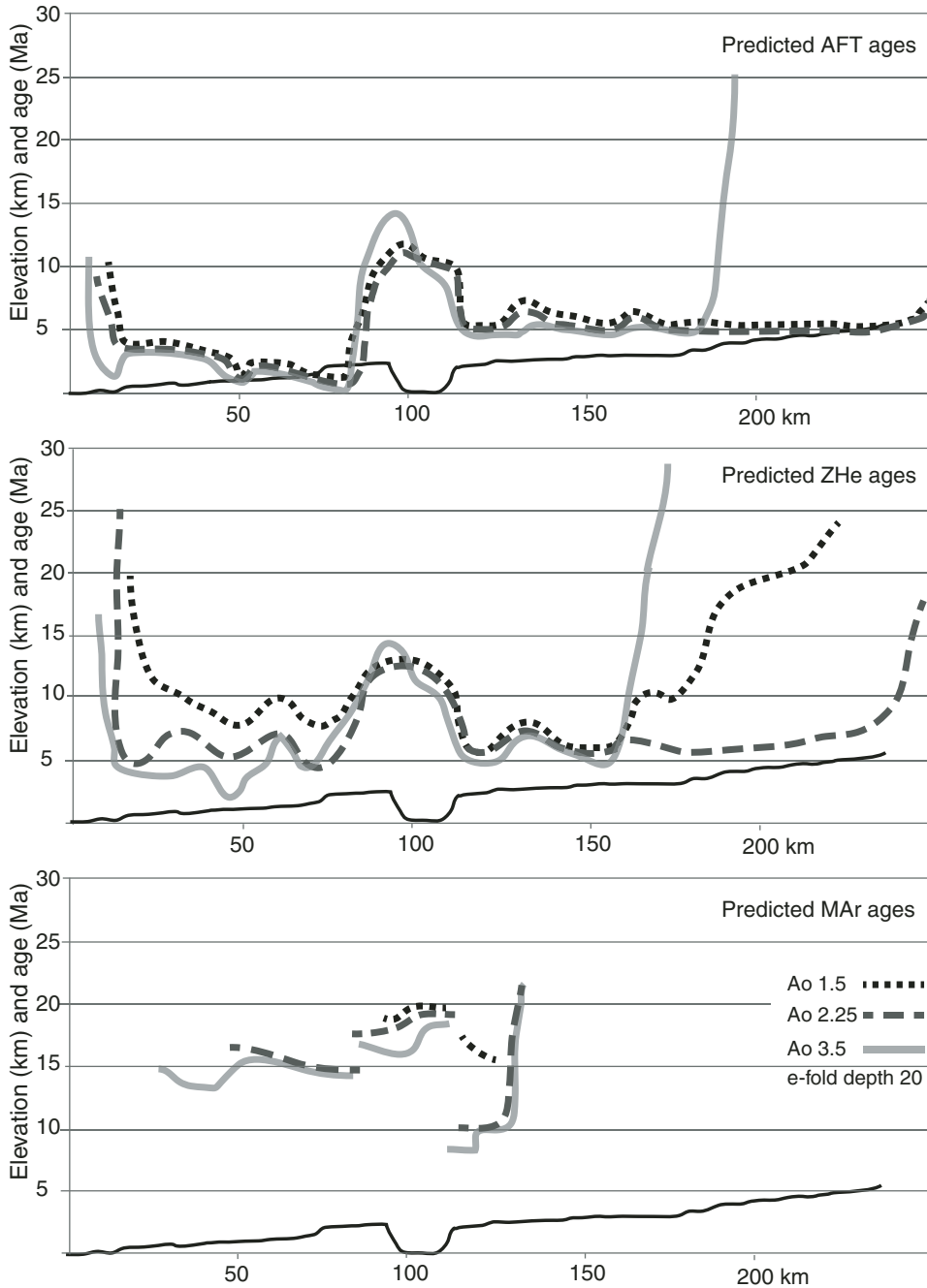


Figure 7. Changes in predicted cooling ages with different radiogenic heat production values (1.5, 2.25, and  $3.5 \mu\text{W m}^{-3}$ ; from McQuarrie and Ehlers, 2015). AFT—apatite fission-track; ZHe—zircon (U-Th)/He; MAR— $^{40}\text{Ar}/^{39}\text{Ar}$  muscovite. Ao is radiogenic heat production and e-fold depth is the depth at which that heat production value exponentially decreases to  $1/e$  of its previous value.

The result is that when the duplex is fully formed (Fig. 8E), the southward-younging pattern is preserved in the ZHe and AFT predicted ages, but the earlier northward-younging cooling signal is preserved in the MAR predicted ages. The abrupt break in cooling ages seen at  $\sim 260$  km in time slice D and at  $\sim 160$  km in time slice E is the result of an out-of-sequence thrust with enough displacement and exhumation to reset AFT, ZHe, and MAR cooling ages (McQuarrie and Ehlers, 2015; Gilmore, 2014). The final times slice, F (Fig. 8), illustrates the predicted ages that would be at the surface today. By looking at the progressive development of the

structures and associated predicted cooling ages, we can see that the complicated across-strike pattern predicted for the three different thermochronometers records cooling associated with four different structural systems: northward migration of a footwall ramp (C), out-of-sequence faulting (D), southward growth of a duplex (D and E), and motion of these structures over two discrete footwall ramps (F). The earlier periods of exhumation are recorded in the higher-temperature chronometers (McQuarrie and Ehlers, 2015), and the most recent pulse of exhumation is recorded by the AFT system.

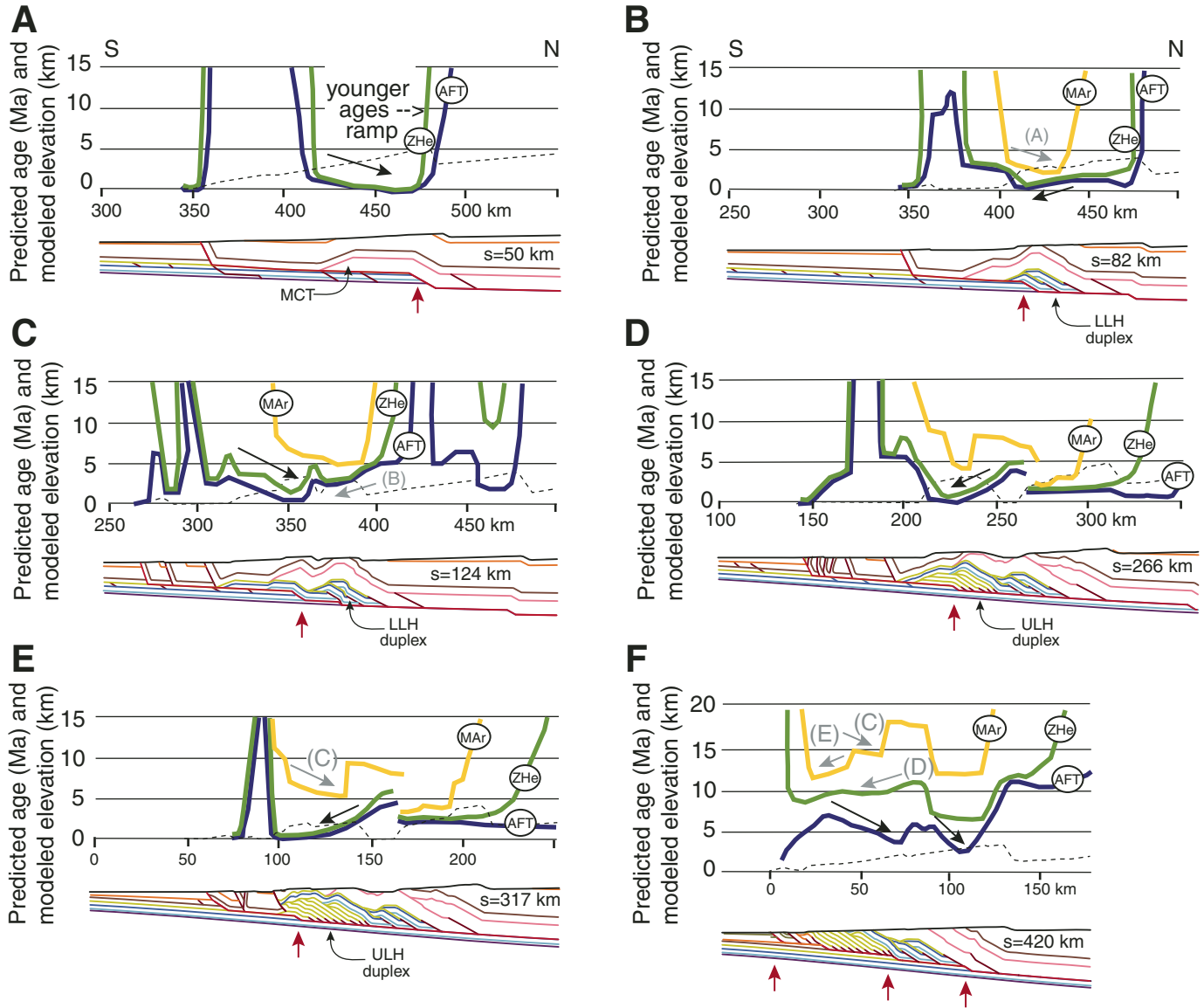


Figure 8. (A–F) Sequentially deformed fold-and-thrust belt (Trashigang section, eastern Bhutan) and associated predicted cooling ages with deformation starting at 20 Ma. AFT—apatite fission-track; ZHe—zircon (U-Th)/He; MAr— $^{40}\text{Ar}/^{39}\text{Ar}$  muscovite; S and N—cardinal directions; MCT—Main Central thrust; LLH—lower Lesser Himalaya; ULH—upper Lesser Himalaya;  $s$ —shortening amount in kilometers. Black arrows indicate active cooling pattern; gray arrows indicate past cooling pattern; the letter in parentheses indicates which panel shows that pulse of cooling; and red arrows indicate positions of active ramps (see text for discussion).

As stated previously in the “Material Properties” section, if the exhumation amount is close to a particular closure temperature depth for a thermochronometric system, then small changes in the magnitude of erosion ( $\sim 1$  km) or changes in the modeled radiogenic heat production value can produce a marked change in the across-strike cooling pattern. For example, using the across-strike cooling patterns illustrated in Figure 8E, a cooler thermal model (using lower radiogenic heat production values) may produce a pattern where only the AFT system is reset with a southward-younging pattern of ages, and the ZHe system retains

the memory of the northward-propagating ramp illustrated in the MAr ages. Another example is illustrated with Figure 8F. A lower modeled radiogenic heat production value, or slightly less erosion, may not produce enough cooling to see the two smaller ramps (red arrows) in the AFT signal. In this scenario, the AFT signal would look similar to the ZHe signal but with slightly younger ages. This example highlights the sensitivity of the crustal thermal field to both the thermophysical properties and boundary conditions used in the thermal model, as well as the structural geometry and kinematics. A prudent approach to

modeling the thermal evolution of a fold-and-thrust belt necessitates a careful evaluation of the ways in which all parameters (both thermal and structural) influence the predicted cooling age. In practice, a proper sensitivity analysis is time consuming, but nevertheless needed.

### Thermal Model Setup Considerations

Setup of a thermal model for simulation of fold-and-thrust belt kinematics and thermochronometer exhumation requires decisions about the type of boundary and initial conditions to assign at the base of the model, and the spatial dimension of the model (e.g., 1-D, 2-D, or three dimensional [3-D]). In the following, we summarize different approaches commonly used and provide some guidelines for consideration in future thermochronometer modeling studies.

Solution of the transient advection diffusion equation in a thermokinematic model necessitates prescribing the boundary conditions (e.g., constant temperature, or constant heat flux) on the sides of the model, as well as the initial temperature condition at which the model starts. Constant temperature boundary conditions are almost always prescribed at the top (Earth) surface of a thermal model because this is typically well known based on meteorological data, as is the change in temperature with elevation (lapse rate) if there is topography in the model. The lateral, or side, thermal boundary conditions are almost always set to a zero flux boundary condition, which means there will be no lateral heat flow (or thermal gradient) at the model side boundaries. The sides of the model must therefore be placed far enough away from the region of interest to avoid influencing temperature gradients where model results are compared to observations.

The basal boundary condition (e.g., at the base of the crust or lithosphere) is less well known and differs between studies. Both constant temperature (e.g., Herman et al., 2010) and constant flux (e.g., Whipp et al., 2007) conditions have been used in previous fold-and-thrust belt studies. The difference between these approaches is that assignment of a constant temperature condition will fix the temperature at the base of the model throughout the simulation, and if care is not taken, this could bias the predicted cooling history of samples exhumed to the surface if they originated from deep in the model. A constant flux boundary basal condition fixes the temperature gradient at the boundary, and it allows temperatures to evolve near the base in response to the imposed kinematics. These two different types of boundary conditions can make a significant difference on predicted lower-crust temperatures. For example, Figure 2 of Herman et al. (2010) shows predicted temperatures across the Himalaya using constant temperature basal boundary conditions. This results in a fixed temperature across the base of the model and influences the geometry of overlying isotherms. In contrast, Figure 3 in Whipp et al. (2007) shows predicted temperatures across the Himalaya using a constant flux boundary condition. In the latter example, temperatures vary across the base of the model in response to the prescribed kinematics. Either approach (constant temperature or

flux) is equally valid and can reproduce surface heat flow that is consistent with observations if the appropriate value for a temperature or flux is chosen. Thus, a critical evaluation of thermal model results requires comparison of results not only to observed cooling ages, but also to available heat-flow determinations from the region to evaluate model consistency with the present-day thermal field. Care should also be taken in evaluating if samples exhumed to the surface in the model originated near the basal boundary where they could have been influenced by the prescribed boundary condition.

A critical step in thermal model setup is identifying how the prescribed basal boundary condition influences (if at all) model interpretations of exhumation and kinematic history. A thorough model setup requires simulation of multiple boundary condition values, and model thicknesses to evaluate if the selected boundary conditions influence the predicted ages. Although many thermal modeling studies select a somewhat shallow depth for the basal boundary condition to decrease computation time (e.g., Herman et al., 2010; Ehlers and Farley, 2003), these values have to be very carefully chosen. Alternatively, if the temperature or thermal gradient at the base of the model is not well known, then a deep (e.g., base of the lithosphere, top of the thermal boundary layer) temperature condition can be chosen (e.g., McQuarrie and Ehlers, 2015). A thicker model domain will unfortunately result in increased computation time.

A final consideration is the spatial dimension to use in the model. Previous fold-and-thrust belt studies reported thermal model results with different spatial dimensions, including 1-D (e.g., Thiede and Ehlers, 2013; Herman et al., 2013; Adams et al., 2015) and more complex 2-D (e.g., Herman et al., 2010; Coutand et al., 2014; McQuarrie and Ehlers, 2015) and 3-D (e.g., Whipp et al., 2007, 2009) models for the Himalaya region. While 3-D models are often appealing if one subscribes to the “more is better” philosophy, they are only needed if the samples interpreted are sensitive to the geometry of the overlying topography (e.g., Braun, 2005; Ehlers and Farley, 2003) and exhumation rates are moderate to slow (e.g.,  $<< 1$  mm/yr as a rule of thumb). Regions with 3-D variations in the geometry of faults and 3-D kinematic fields also warrant use of a 3-D model, if samples were collected to detect these variations. If the region of interest has rapid exhumation (e.g.,  $> 1$  mm/yr), such as in the Himalaya or Taiwan, then the subsurface thermal gradients will be high and laterally constant across valleys and ridges. This lateral consistency means that any lateral variations in temperature due to topography are small because they are overwhelmed by the effect of erosion on the thermal gradient. As a result, for thermochronometer systems with closure temperatures  $< 300$  °C, a 1-D thermal model is often sufficient to quantify exhumation rates in rapidly exhuming regions (see discussions in Whipp et al., 2007; Thiede and Ehlers, 2013). However, in regions where exhumation rates are slower (e.g.,  $< 1$  mm/yr), the lower-temperature thermochronometer systems will be more sensitive to thermal gradient perturbations due to topography or lateral motion due to faults. This is why paleotopography studies using thermochronometer data are often most

successfully completed in areas with moderate to slow exhumation rates (e.g., House et al., 1998; Ehlers et al., 2006; Olen et al., 2012). For the Himalaya, previous 1-D models have focused on interpreting exhumation rates from low-temperature thermochronometer systems mainly from the rapidly exhuming Greater Himalaya region. This setting has high exhumation rates (typically >2 mm/yr), and, as such, a 1-D modeling approach is defensible (see discussion in Thiede and Ehlers, 2013). In contrast, the model results presented in this manuscript for the Himalaya fold-and-thrust belt are 2-D. The motivation for using a 2-D approach here is that many of the samples analyzed in fold-and-thrust belts are partially reset or unreset, or they have experienced cooling through closure temperature depths a significant lateral distance away (e.g., above a ramp) from the point of final erosional exhumation to the surface. Thus, when trying to interpret the lateral and vertical kinematic history of a fold-and-thrust belt with samples spanning a large range of ages and significant lateral displacement, a 2-D model is warranted, and a 1-D model would be insufficient. In summary, the choice of the spatial dimension to use in a model (i.e., 1-D vs. 2-D or 3-D) depends on the scientific questions being asked and where the data were collected, as well as the specific tectonic setting. Although many geoscientists model data following the collection of samples, it is often advisable to set up simple models of an area prior to collecting thermochronometer data to see if the intended sampling approach can capture the signal necessary to evaluate their hypothesis.

## DISCUSSION AND CONCLUSIONS

### Drivers of Thermochronometer Age Patterns

The cooling ages shown from across a range of orogens depicted in Figure 5 highlight both broad similarities among the patterns as well as some key differences. A natural question arising from these plots is: What do the pattern and range of cooling ages mean? At the largest scale, we can examine whether the pattern of ages can be modeled as continuous particle paths at the scale of the orogen. We can evaluate two different large-scale patterns of material added to the orogen. The first scenario is one where accretion is focused in the rear of the orogen due to the location of a ramp in the décollement and the associated duplexing (modeled as a zone of focused accretion) of material (Fig. 2). The narrowness of this zone and the rate of accretion determine the steepness of the particle paths and magnitude of exhumation (e.g., Fuller et al., 2006b). The second scenario is one in which the orogen grows outward with time, and the zone of focused accretion and erosion (controlled by a steep increase in topography) steps outward as well (e.g., Reiners et al., 2015). For scenario one, the predicted age pattern is one in which the ages decrease toward the hinterland, where there is a zone of focused accretion/erosion (Fig. 2). This pattern is most readily seen in the age-distance relationship of thermochronometers in central Nepal and, to a first order, in central Taiwan (Figs. 5C and 5D). The second scenario predicts a pattern of cooling ages that

young toward the foreland with time, with the slope of the age-distance relationship being a direct result of the age of outward fault propagation (Reiners et al., 2015). This large-scale pattern of younger ages toward the foreland is apparent in the age-distance trend of thermochronometers in the Andes of northern Argentina (23°–27°S; Fig. 5F), and it includes the foreland basement uplifts (Pearson et al., 2013; Reiners et al., 2015). However, these trends of younging ages toward the hinterland or younging toward the foreland are not apparent in either of the age-distance transects across Bhutan or the age-distance transect across Bolivia. In detail, there are also ages that notably fall off of the orogen-scale trend in Taiwan (between 70 and 90 km from the deformation front) and Argentina (Fig. 5). In Argentina, while the youngest AFT and apatite (U-Th)/He (AHe) data define a younging toward the foreland trend, there are at least two pronounced gaps in this pattern. One gap is between 325 and 450 km from the deformation front, and a second is between 150 and 275 km from the deformation front (Fig. 5F). In both of these regions, the lack of young ages is not a function of sampling density, but rather it indicates that the sample chronometers are notably older. Thus, if we were to connect the AFT ages in a way that would mimic a line of predicted ages similar to those shown in Figure 8, we would see a rapid decrease in age from unreset to reset ages at 150 km. These ages would then increase to match the 80–100 Ma ages from 175 to 225 km before decreasing in age again to match the suite of ca. 20 Ma reset ages from 225 to 325 km. The AFT data again increase significantly in age (from 50 to 200 Ma) between 350 and 450 km from the deformation front. At 450 km, the ages are again young (20 Ma) and show a gentle increase in age from 20 Ma to 50 Ma over the next 100 km (Fig. 5F).

The pattern of young reset ages interspersed with older reset or unreset ages is the most apparent pattern of ages in the Bolivian Andes (Fig. 5E). Here, young (ca. 10 Ma) ages at 100 km and again at 160–190 km from the deformation front are separated by zones of unreset (ages > 70 Ma) or ages that were reset much earlier in the deformation history (ca. 45 Ma). Also, similar to Argentina, there is a narrow zone (160–180 km from the deformation front) where significantly more exhumation has occurred to also reset ZFT and <sup>40</sup>Ar/<sup>39</sup>Ar (mica and feldspar) ages. In Argentina, this area of high exhumation is at ~100 km and is one of the few places that displays reset ZHe ages. The patterns of young reset and partially reset ages in Bolivia have been explained by the location of active uplift, active uplift along ramps that cut through sedimentary rocks in the Subandes (40–50 km), and active uplift over ~10 km basement hanging-wall (~100 km from the deformation front) and footwall (~160–180 km from the deformation front) ramps (Rak, 2015; Fig. 5E).

Although the orogen-scale motion of material through a critical wedge (Fig. 2) may adequately reproduce the spatial patterns of cooling ages across some fold-and-thrust belts (Willett and Brandon, 2002; Fuller et al., 2006b; Herman et al., 2010; Thomson et al., 2010), increasingly more densely spaced thermochronologic data across a greater number of orogens highlight patterns of cooling ages that have wavelengths of ~20–100 km

and amplitudes (for any given thermochronometer) that can be resolved as low as 3–5 m.y. These patterns, which are significantly more narrow than the scale of an orogen, are a function of active or formerly active structures, notably ramps in the décollement (Fig. 8). As discussed in the section on “Thrust Systems,” the pattern of cooling ages at the surface (Figs. 5 and 8F) contains information about not only the active structures that induced exhumation, but also the history of exhumation associated with previous structures (e.g., McQuarrie and Ehlers, 2015). When well resolved by thermochronometer data, the cooling history of the rocks preserved in the sampled thermochronometers may record the growth and propagation of specific thrust belt structures such as fault bend folds, duplexes, and imbricate fans elucidated through coeval deformation and erosion. This detailed record preserved in a suite of chronometers can be identified through thermochronometric sampling over a broad, across-strike area in a fold-and-thrust belt, and it can be used to identify the geometry of active and inactive structures (particularly the positions of ramps with time) as well as the rates at which these faults have moved through time (McQuarrie and Ehlers, 2015; Rak, 2015; Gilmore, 2014).

We note, however, that the sensitivity of thermochronometric ages to record activity on individual structures in fold-and-thrust belts depends on the age of deformation. The examples provided in Figure 5 and discussed herein are all cases where deformation is Cenozoic in age, and, in many cases, is still active today. These types of studies are preferred if the intent of using thermochronometer data is to understand the kinematics of individual structures or regions of a fold-and-thrust belt. The reason for this is that thermochronometer ages commonly have uncertainties that are ~10%–20% (e.g., Fosdick et al., 2015) of the age measured. If individual thrust sheets are active for 5–10 m.y. before deformation migrates elsewhere, then the uncertainties on ages used in an analysis will need to be less than this amount of time if information about the kinematics of the structures is desired. This implies that Cenozoic fold-and-thrust belts are the best target for the type of analysis presented in Figures 6 and 8. Thus, recently active structures have a better chance of retaining a signal of the fault kinematics than will, for example, a ca. 300 Ma Paleozoic thrust belt, which might have uncertainties in ages of ~30–60 m.y. that will mask the timing of individual thrust sheet activity.

### **Sensitivity of Thermal Fields and Thermochronometers to Subsurface Structures**

While rocks record cooling associated with every component of structurally induced exhumation, the uplift and exhumation that are recorded by any given thermochronometer are dependent upon the magnitude of exhumation associated with displacement on a structure and the thermal history of the rocks: length and magnitude of burial, speed of exhumation, and heat production. If the magnitude of exhumation is particularly close to that necessary to reset a thermochronometer system, the predicted pattern of cooling ages can be significantly altered by small changes

in modeled topography or heat production. Thus, changing the location of small (~2-km-high) footwall ramps may have very modest implications that could be obscured by changes in modeled topography or modeled heat production values. However, the larger the ramp, the more significant is the vertical component of the velocity field and the more robust is its cooling signal. A 5-km-high footwall ramp will have a signal that is seen in a 5–10 m.y. difference in ages between the reset ages that have been uplifted and exhumed over the ramp (Fig. 8) and those that have not (McQuarrie and Ehlers, 2015; Gilmore, 2014). A large footwall ramp, such as the 10-km-high basement ramps proposed for the Bolivian Andes (McQuarrie, 2002a; McQuarrie et al., 2008), would produce a dramatic cooling age signal, where the age offset over the ramp would extend from not reset to reset, or would display an age difference of 30–40 m.y. (Rak, 2015).

### **Can Thermochronometers Aid in Constructing More Viable Balanced Sections?**

Balanced cross sections provide a direct model of the subsurface geometry that can reproduce the mapped surface geology, and they require that the lengths and locations of hanging-wall and footwall ramps match. As a result, these balanced cross sections provide a viable, possible, kinematic progression of deformation as well as a template of the ways in which the location and magnitude of ramps in the basal décollement have evolved with time. However, even when matching the surface geology, and all available geophysical constraints, cross sections are still considered the “best guess” for the proposed subsurface geometry and may permit multiple interpretations of proposed subsurface structures, décollement ramp locations, and total shortening estimates. We suggest that the integration of cross sections with thermochronometers has the power to provide a quantitative test of the validity of balanced cross-section geometry and kinematics because of the strong relationship between the location of ramps or zones of accretion, which provide the vertical component of the kinematic field, and young predicted cooling ages recorded at the surface in rapidly eroding orogens (e.g., Fuller et al., 2006b; Whipp et al., 2007; Robert et al., 2011; Coutand et al., 2014). If the geometry (i.e., locations of ramps proposed in the balanced section) cannot predict the measured ages (using a suite of rates and thermal properties), then that geometry is not valid, even if it does balance in a traditional sense (McQuarrie and Ehlers, 2015). Thus, cooling ages have the potential to test the viability of proposed cross-section kinematics and highlight regions where the cross-section geometry needs to be altered to match the cooling ages (Gilmore, 2014). Gilmore (2014) showed that the cooling ages predicted from two different cross-section geometries were notably different, particularly in modeled AFT ages (Fig. 9). The predicted ages from the original cross-section geometry (Long et al., 2011b) reflected a cooling signal imparted by a large 5 km ramp that produced a marked change (from south to north) from young ages, reset by uplift over the ramp, to older ages that were reset earlier in the deformation history (Fig. 9A).

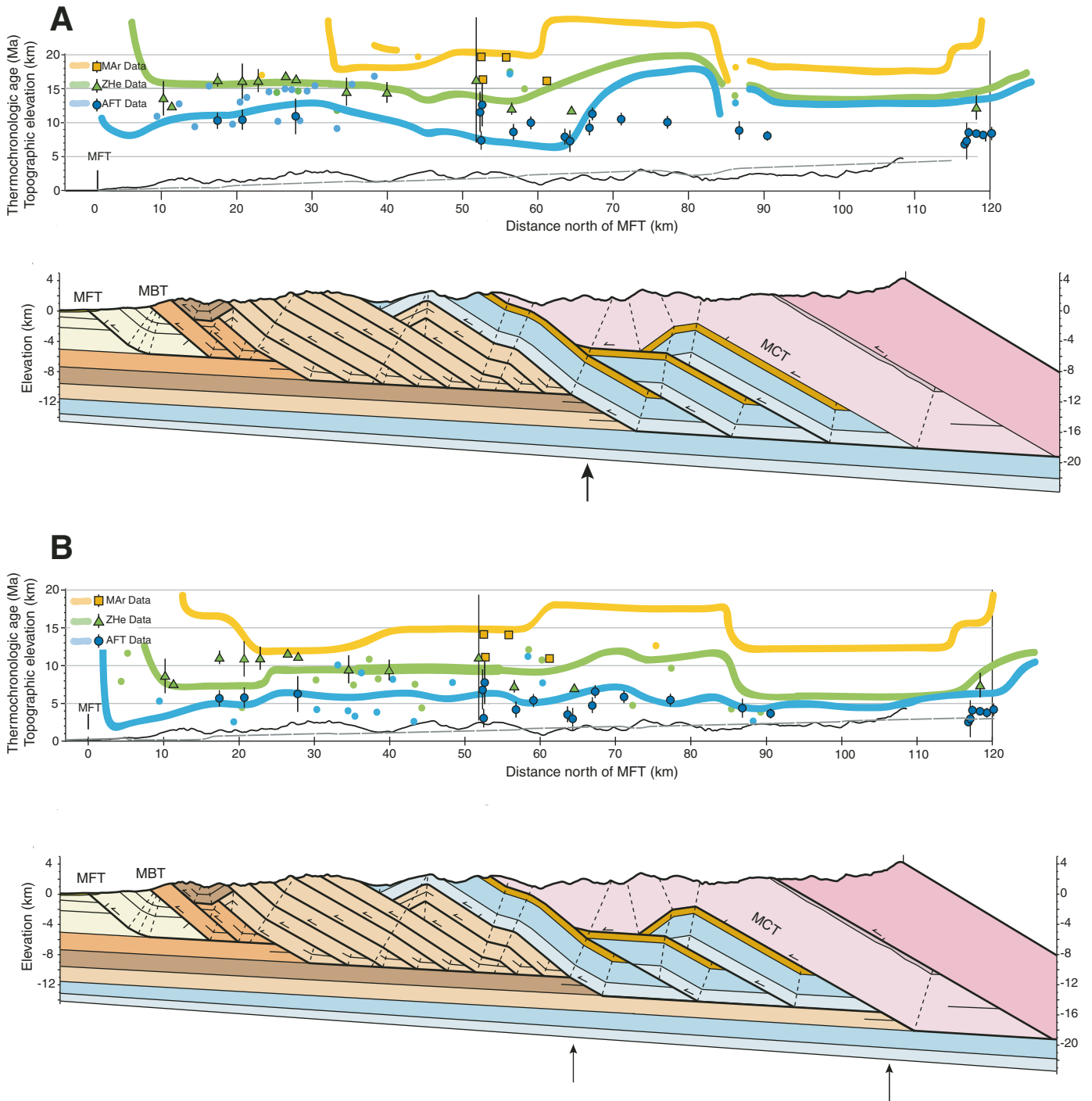


Figure 9. Balanced cross section and plot of thermochronometric data vs. distance from Main Frontal thrust (MFT) projected above the line from the Trashigang region of eastern Bhutan (Long et al., 2011b). Yellow squares— $^{40}\text{Ar}/^{39}\text{Ar}$  muscovite (MAR) data; green triangles—zircon (U-Th)/He (ZHe) data; and blue circles—apatite fission-track (AFT) data. Data are from Long et al. (2012), and Coutand et al. (2014). Thin black vertical bars represent  $2\sigma$  error. Thick colored lines represent thermokinematic predicted MAR ages (yellow), ZHe ages (green), and AFT ages (blue). (A) Original geometry from Long et al. (2011b). Arrow highlights location of active footwall ramp. Note mismatch between predicted and measured AFT thermochronometric ages between 60 and 90 km from Main Frontal thrust. MBT—Main Boundary thrust; MCT—Main Central thrust. (B) Revised geometry of cross section. Arrows represent new ramp locations, and the blue line representing AFT predicted ages intersects more of the measured AFT ages.

These predicted ages did not match the measured ages, which continued to young to the north between 60 and 90 km from the Main Frontal thrust (Gilmore, 2014). Breaking the large ramp into two smaller ramps that are offset by 50 km, with the northern ramp located as far north as the reset ages, resulted in a different pattern of predicted ages, which continued to young to the north and matched the trend of published data (Fig. 9B). Both versions of the cross section balance in the traditional sense; however, the second version is more viable because it can produce predicted thermochronometer ages that match measured ages through the region (Gilmore, 2014).

## Implications for Advances in Tectonics

### Rates of Deformation

Accurate determination of the geometry, magnitude, and rates of shortening in convergent systems has far-reaching implications for assessing both the drivers and expected responses of geodynamic processes and thus for discovering new and intriguing research questions. The advent and growth of high-resolution global positioning system (GPS) data sets have provided unprecedented resolution on modern rates of motion across faults. How do these modern rates correlate with long-term ( $10^7$  yr) displacement rates or fault rates calculated over  $10^3$  yr via cosmogenic nuclide dating (e.g., Lavé and Avouac, 2000)? If the long-term rates are shown to vary over  $10^7$  yr, as has been suggested (Long et al., 2012; McQuarrie and Ehlers, 2015; Pană and van der Pluijm, 2015), what are the processes driving that change? For example, several studies have sought for correlations between age and rate of shortening in fold-and-thrust belts and paleo-altimetry data suggesting attainment of high topography. Both the Himalayan and the Andean fold-and-thrust belts are adjacent to orogenic plateaus. Researchers have proposed both slow and steady attainment of elevation, commensurate with shortening (Barnes and Ehlers, 2009; DeCelles et al., 2007), and rapid elevation gain due to delamination of a dense lithospheric root (e.g., Garzzone et al., 2006; Molnar and Stock, 2009). The predicted response to a rapid change of elevation and thus supercritical wedge conditions is a rapid outward propagation of the fold-and-thrust belt and a potential increase in shortening rates (e.g., Garzzone et al., 2006; DeCelles et al., 2009), information that has previously been unavailable.

### Linking Deformation Rates to Rates of Surface Processes

The methods presented here for integrating the geometry of structures and rates of shortening, and predicting the resulting topographic, basin, and erosional response to those structures and rates allow for quantitative links between surface and subsurface processes.

Previously, research attempting to quantify the rates of shortening could only broadly relate displacement on a suite of structures to the measured cooling ages (Elger et al., 2005; McQuarrie et al., 2008; Long et al., 2012; Thiede et al., 2009) or foreland basin deposits (DeCelles et al., 1995; Jordan et al.,

2001). Well-dated growth structures (Lawton et al., 1993; Jordan et al., 1993; Horton, 1998; Perez and Horton, 2014) provide critical constraints on the end of fault motion, but they rarely limit age of fault initiation. As mentioned in the previous subsection, linking cross-section estimates of shortening with thermokinematic models allows for the quantification of shortening rates as well as evaluation of the uniqueness of those rates (McQuarrie and Ehlers, 2015; Rak, 2015). This is critical for studies that seek to integrate deformation, uplift, and erosion rates and identify potential lags in the system (Thiede et al., 2009; Val et al., 2016; Adams et al., 2016). As highlighted in the “Thrust Systems” section, a cooling age, particularly in a system of stacked thrusts and thrust ramps, may not be representative of the age of motion on the structure from which it was collected. In addition, isostatic loads, which affect the magnitude and extent of basin deposits, may not be limited to the frontal thrust structures, highlighting the need for an integrated approach. With the growing ability to mine topographic data sets to ascertain the spatial and temporal patterns of differential uplift of rock (e.g., Wobus et al., 2006; Kirby and Whipple, 2012), the geomorphic signal of rock uplift can also be quantitatively tied to the geometry and displacement history of structures producing that uplift. We would argue that the reconstructed history of cross-section deformation must be consistent with the rate, timing, and geometry of rock uplift inferred independently from geomorphic analyses, cosmogenic radionuclide erosion rate patterns determined from cosmogenic nuclide dating (e.g., Adams et al., 2016; Val et al., 2016), and thermochronometric cooling age patterns. The velocity input into thermokinematic models such as Pecube used to predict cooling ages (see “Thermal Structure of Fold-and-Thrust Belts” section) can also be input into planform surface models, such as CASCADE, which simulated an evolving river network with trunk streams and interfluvies, facilitating direct comparisons of predicted and measured geomorphic indicators.

## SUMMARY

Fold-and-thrust belts and their associated foreland basins provide a record of deformation, exhumation, and sedimentation of past and present contractional orogenic systems. The growing ability to combine geologic data (maps and cross sections), geochemical data (geothermometers, geochronometers, geobarometers, and thermochronometers), and geophysical techniques, such as numerical modeling, has an enormous potential to quantify the rates, magnitudes, and timing of deformation and erosion in active, contractional settings. The interpretation of thermochronometric data in these contractional settings is dependent on the thermal, kinematic, and erosion history of the sampled rocks. We assert that the geometry of fold-and-thrust belts, as delineated through balanced cross sections, provides a series of testable kinematics scenarios that, when combined with a subsurface thermal field from a thermal model, can be used to calculate thrust belt displacement, velocity, acceleration/deceleration, and the associated pattern and magnitude of erosion. The resulting

deformation history will provide insight into previously elusive long-term displacement fields of continental deformation in convergent orogenic systems.

## ACKNOWLEDGMENTS

This research was supported by an Alexander von Humboldt Foundation fellowship to McQuarrie to collaborate with Ehlers at the University of Tübingen in Germany, as well as National Science Foundation grants EAR-0738522 and NSF-1524277 to N. McQuarrie and a European Research Council consolidator grant (ERC-CoG 615703) to Ehlers. We acknowledge and thank Midland Valley for support and use of the program Move, Willi Kappler (University of Tübingen) for his time and programming assistance, and Michelle Gilmore, Adam Rak, and Ashley Ace for insightful comments, discussion, and figures. Insights, edits, and suggestions from Julie Fosdick, an anonymous reviewer, and Editor Ryan Thigpen improved the presentation and impact of this paper.

## REFERENCES CITED

- Adam, J., Klaeschen, D., Kukowski, N., and Flueh, E., 2004, Upward delamination of the Cascadia Basin sediment infill with landward frontal accretion thrusting caused by rapid glacial age material flux: *Tectonics*, v. 23, TC3009, doi:10.1029/2002TC001475.
- Adams, B.A., Hodges, K.V., van Soest, M.C., and Whipple, K.X., 2013, Evidence for Pliocene–Quaternary normal faulting in the hinterland of the Bhutan Himalaya: *Lithosphere*, v. 5, p. 438–449, doi:10.1130/L277.1.
- Adams, B.A., Hodges, K.V., Whipple, K.X., Ehlers, T.A., van Soest, M.C., and Wartho, J., 2015, Constraints on the tectonic and landscape evolution of the Bhutan Himalaya from thermochronometry: *Tectonics*, v. 34, p. 1329–1347, doi:10.1002/2015TC003853.
- Adams, B.A., Whipple, K.X., Hodges, K.V., and Heimsath, A.M., 2016, In situ development of high-elevation, low-relief landscapes via duplex deformation in the Eastern Himalayan hinterland, Bhutan: *Journal of Geophysical Research—Earth Surface*, v. 121, p. 294–319, doi:10.1002/2015JF003508.
- Allmendinger, R.W., and Gubbels, T., 1996, Pure and simple shear plateau uplift, Altiplano-Puna, Argentina and Bolivia: *Tectonophysics*, v. 259, p. 1–13, doi:10.1016/0040-1951(96)00024-8.
- Allmendinger, R.W., Jordan, T.E., Kay, S.M., and Isacks, B.L., 1997, The evolution of the Altiplano-Puna plateau of the Central Andes: *Annual Review of Earth and Planetary Sciences*, v. 25, p. 139–174, doi:10.1146/annurev.earth.25.1.139.
- Aoki, Y., Ikawa, T., Ohta, Y., and Tamano, T., 1982, Compressional wave velocity analyses for suboceanic basement reflectors in the Japan Trench and Nankai Trough based on multichannel seismic reflection profiles, *in* Hilde, W.C., and Uyeda, S., eds., *Geodynamics of the Western Pacific–Indonesian Region*: American Geophysical Union Geodynamic Monograph 11, p. 355–370, doi:10.1029/GD011p0355.
- Avouac, J.P., 2003, Mountain building, erosion, and the seismic cycle in the Nepal Himalaya: *Advances in Geophysics*, v. 46, p. 1–80, doi:10.1016/S0065-2687(03)46001-9.
- Baby, P., Limachi, R., Moretti, I., Mendez, E., Oller, J., Guiller, B., and Specht, M., 1995, Petroleum system of the northern and central Bolivian sub-Andean zone, *in* Tankard, A.J., Suarez, R., and Welsink, H.J., eds., *Petroleum Basins of South America*: American Association of Petroleum Geologists Memoir 62, p. 445–458.
- Bally, A.W., Gordy, P.L., and Stewart, G.A., 1966, Structure, seismic data, and orogenic evolution of southern Canadian Rocky Mountains: *Bulletin of Canadian Petroleum Geology*, v. 14, p. 337–381.
- Barker, C.E., 1988, Geothermics of petroleum systems: Implications of the stabilization of kerogen thermal maturation after a geologically brief heating duration at peak temperature, *in* Magoon, L.B., ed., *Petroleum Systems of the United States*: U.S. Geological Survey Bulletin 1870, p. 26–29.
- Barnes, J.B., and Ehlers, T.A., 2009, End member models for Andean Plateau uplift: *Earth-Science Reviews*, v. 97, p. 105–132, doi:10.1016/j.earscirev.2009.08.003.
- Barnes, J.B., Ehlers, T.A., McQuarrie, N., O’Sullivan, P.B., and Pelletier, J.D., 2006, Variations in Eocene to recent erosion across the central Andean fold-thrust belt, northern Bolivia: Implications for plateau evolution: *Earth and Planetary Science Letters* v. 248, p. 118–133, doi:10.1016/j.epsl.2006.05.018.
- Barnes, J.B., Ehlers T.A., Insel, N., McQuarrie, N., and Poulsen, C.J., 2012, Linking orography, climate, and exhumation across the central Andes: *Geology*, v. 40, p. 1135–1138, doi:10.1130/G33229.1.
- Barr, T.D., and Dahlen, F.A., 1989, Brittle frictional mountain building 2. Thermal structure and heat budget: *Journal of Geophysical Research*, v. 94, p. 3923–3947, doi:10.1029/JB094iB04p03923.
- Batt, G.E., Brandon, M.T., Farley, K.A., and Roden-Tice, M., 2001, Tectonic synthesis of the Olympic Mountains segment of the Cascadia wedge, using two-dimensional thermal and kinematic modeling of thermochronological ages: *Journal of Geophysical Research*, v. 106, p. 26,731–26,746, doi:10.1029/2001JB000288.
- Beaumont, C., 1978, The evolution of sedimentary basins on a viscoelastic lithosphere: Theory and examples: *Royal Astronomical Society Geophysical Journal*, v. 55, p. 471–497, doi:10.1111/j.1365-246X.1978.tb04283.x.
- Beaumont, C., 1981, Foreland basins: *Royal Astronomical Society Geophysical Journal*, v. 65, p. 291–329, doi:10.1111/j.1365-246X.1981.tb02715.x.
- Beaumont, C., Fullsack, P., and Hamilton, J., 1992, Erosional control of active compressional orogens, *in* McClay, K.R., ed., *Thrust Tectonics*: New York, Chapman and Hall, p. 1–18, doi:10.1007/978-94-011-3066-0\_1.
- Behrmann, J.H., Brown, K., Moore, J.C., Mascare, A., Taylor, E., Alvarez, F., Andreieff, P., Barnes, R., Beck, C., Blanc, G., Clark, M., Dolan, J., Fisher, A., Gieskes, J., Hounslow, M., McLellan, P., Moran, K., Ogawa, Y., Sakai, T., Schoonmaker, J., Vrolijk, P., Wilkens, R., and Williams, C., 1988, Evolution of the structures and fabrics in the Barbados accretionary prism: Insights from Leg 110 of the Ocean Drilling Program: *Journal of Structural Geology*, v. 10, p. 577–591, doi:10.1016/0191-8141(88)90025-9.
- Bendick, R., and Ehlers, T.A., 2014, Extreme localized exhumation at syntaxes initiated by subduction geometry: *Geophysical Research Letters*, v. 41, p. 5861–5867, doi:10.1002/2014GL061026.
- Benjamin, M.T., Johnson, N.M., and Naeser, C.W., 1987, Recent rapid uplift in the Bolivian Andes: Evidence from fission-track dating: *Geology*, v. 15, p. 680–683, doi:10.1130/0091-7613(1987)15<680:RRUITB>2.0.CO;2.
- Bernstein-Taylor, B.L., Kirchoff-Stein, K.S., Silver, E.A., Reed, D.L., and Mackay, M., 1992, Large-scale duplexes within the New Britain accretionary wedge: A possible example of accreted ophiolitic slivers: *Tectonics*, v. 11, p. 732–752, doi:10.1029/91TC02901.
- Beutner, E.C., 1977, Causes and consequences of curvature in the Sevier orogenic belt, Utah to Montana, *in* Rocky Mountain Thrust Belt Geology and Resources: Wyoming Geological Association 29th Annual Field Conference Guidebook, p. 353–365.
- Beysac, O., Bollinger, L., Avouac, J.P., and Goffe, B., 2004, Thermal metamorphism in the Lesser Himalaya of Nepal determined from Raman spectroscopy of carbonaceous material: *Earth and Planetary Science Letters*, v. 225, p. 233–241, doi:10.1016/j.epsl.2004.05.023.
- Bollinger, L., Henry, P., and Avouac, J.P., 2006, Mountain building in the Nepal Himalaya: Thermal and kinematic model: *Earth and Planetary Science Letters*, v. 244, p. 58–71, doi:10.1016/j.epsl.2006.01.045.
- Boyer, S.E., 1995, Sedimentary basin taper as a factor controlling the geometry and advance of thrust belts: *American Journal of Science*, v. 295, p. 1220–1254, doi:10.2475/ajs.295.10.1220.
- Boyer, S.E., and Elliott, D., 1982, Thrust systems: *American Association of Petroleum Geologists Bulletin*, v. 66, p. 1196–1230.
- Brady, R.J., Duce, M.N., Kidder, S.J., and Saleeby, J.B., 2006, The distribution of radiogenic heat production as a function of depth in the Sierra Nevada batholith, California: *Lithos*, v. 86, p. 229–244, doi:10.1016/j.lithos.2005.06.003.
- Brandon, M.T., and Vance, J.A., 1992, Tectonic evolution of the Cenozoic Olympic subduction complex, Washington State, as deduced from fission-track ages for detrital zircons: *American Journal of Science*, v. 292, p. 565–636, doi:10.2475/ajs.292.8.565.
- Brandon, M.T., Roden-Tice, M.K., and Garver, J.I., 1998, Late Cenozoic exhumation of the Cascadia accretionary wedge in the Olympic Mountains, northwest Washington State: *Geological Society of America Bulletin*,

- v. 110, p. 985–1009, doi:10.1130/0016-7606(1998)110<0985:LCEOTC>2.3.CO;2.
- Braun, J., 2002, Quantifying the effect of Recent relief changes on age-elevation relationships: *Earth and Planetary Science Letters*, v. 200, p. 331–343, doi:10.1016/S0012-821X(02)00638-6.
- Braun, J., 2005, Quantifying constraints on the rate of landform evolution derived from low-temperature thermochronology, in Reiners, P.W., and Ehlers, T.A., eds., *Low-Temperature Thermochronology: Techniques, Interpretations, and Applications*: Mineralogical Society of America Reviews in Mineralogy and Geochemistry, v. 58, p. 351–374, doi:10.2138/rmg.2005.58.13.
- Bray, J.C., and Karig, D.E., 1988, Dewatering and extensional deformation of the Shikoku Basin hemipelagic sediments in the Nankai Trough: *Pure and Applied Geophysics*, v. 128, p. 725–747, doi:10.1007/BF00874554.
- Brewer, J., 1981, Thermal effects of thrust faulting: *Earth and Planetary Science Letters*, v. 56, p. 233–244, doi:10.1016/0012-821X(81)90130-8.
- Brown, W.G., 1988, Deformational style of Laramide uplifts in the Wyoming foreland, in Schmidt, C.J., and Perry, W.J., eds., *Interaction of the Rocky Mountain Foreland and the Cordilleran Thrust Belt*: Geological Society of America Memoir 171, p. 1–26, doi:10.1130/MEM171-p1.
- Burbank, D.W., Puigdefabregas, C., and Munoz, J.A., 1992, The chronology of the Eocene tectonic and stratigraphic development of the eastern Pyrenean foreland basin, northeast Spain: *Geological Society of America Bulletin*, v. 104, p. 1101–1120, doi:10.1130/0016-7606(1992)104<1101:TCOTET>2.3.CO;2.
- Carrapa, B., Trimble, J.D., and Stockli, D.F., 2011, Patterns and timing of exhumation and deformation in the Eastern Cordillera of NW Argentina revealed by (U-Th)/He thermochronology: *Tectonics*, v. 30, TC3003, doi:10.1029/2010TC002707.
- Carslaw, H.S., and Jaeger, J.C., 1959, *Conduction of Heat in Solids* (2nd ed.): Oxford, UK, Oxford University Press, 520 p.
- Castaño, J.R., and Sparks, D.M., 1974, Interpretations of vitrinite reflectance measurement in sedimentary rocks and determination of burial history using vitrinite reflectance and authigenic minerals, in Dutcher, R.R., ed., *Carbonaceous Minerals as Indicators of Metamorphism*: Geological Society of America Special Paper 153, p. 31–52, doi:10.1130/SPE153-p31.
- Catuneanu, O., 2004, Retroarc foreland systems—Evolution through time: *Journal of African Earth Sciences*, v. 38, p. 225–242, doi:10.1016/j.jafrearsci.2004.01.004.
- Chapman, D., 1986, Thermal gradients in the continental crust, in Dawson, J.B., Carswell, D.A., Hall, J., and Wedepohl, K.H., eds., *The Nature of the Lower Continental Crust*: Geological Society, London, Special Publication 24, p. 63–70.
- Chapple, W.M., 1978, Mechanics of thin-skinned fold-and-thrust belts: *Geological Society of America Bulletin*, v. 89, p. 1189–1198, doi:10.1130/0016-7606(1978)89<1189:MOTFB>2.0.CO;2.
- Chase, C.G., 1992, Fluvial landscape and the fractal dimension of topography: *Geomorphology*, v. 5, p. 39–57, doi:10.1016/0169-555X(92)90057-U.
- Cloos, M.L., 1982, Flow mélanges: Numerical modeling and geologic constraints on their origin in the Franciscan subduction complex, California: *Geological Society of America Bulletin*, v. 93, p. 330–345, doi:10.1130/0016-7606(1982)93<330:FMNMG>2.0.CO;2.
- Cooper, F.J., Hodges, K.V., and Adams, B.A., 2013, Metamorphic constraints on the character and displacement of the South Tibetan fault system, central Bhutanese Himalaya: *Lithosphere*, v. 5, p. 67–81, doi:10.1130/L221.1.
- Costa, E., and Vendeville, B.C., 2002, Experimental insights on the geometry and kinematics of fold-and-thrust belts above weak, viscous evaporitic décollement: *Journal of Structural Geology*, v. 24, p. 1729–1739, doi:10.1016/S0191-8141(01)00169-9.
- Coutand, I., Whipp, D.M., Jr., Grujic, D., Bernet, M.B., Fellin, M.G., Bookhagen, B., Landry, K.R., Ghalley, S.K., and Duncan, C., 2014, Geometry and kinematics of the Main Himalayan thrust and Neogene crustal exhumation in the Bhutanese Himalaya derived from inversion of multi-thermochronologic data: *Journal of Geophysical Research—Solid Earth*, v. 119, p. 1446–1481, doi:10.1002/2013JB010891.
- Coyle, D.A., and Wagner, G.A., 1998, Positioning the titanite fission-track partial annealing zone: *Chemical Geology*, v. 149, p. 117–125, doi:10.1016/S0009-2541(98)00041-2.
- Cross, E., III, 2014, *The Structure, Stratigraphy, and Evolution of the Lesser Himalaya of Central Nepal* [M.S. thesis]: Tucson, Arizona, University of Arizona, 97 p.
- Dahl, P.S., 1996, The effects of composition on retentivity of argon and oxygen in hornblende and related amphiboles: A field-tested empirical model: *Geochimica et Cosmochimica Acta*, v. 60, p. 3687–3700, doi:10.1016/0016-7037(96)00170-6.
- Dahlen, F.A., 1990, Critical taper model of fold-and-thrust belts and accretionary wedges: *Annual Review of Earth and Planetary Sciences*, v. 18, p. 55–99, doi:10.1146/annurev.earth.18.050190.000415.
- Dahlen, F.A., Suppe, J., and Davis, D., 1984, Mechanics of fold-and-thrust belts and accretionary wedges: Cohesive Coulomb theory: *Journal of Geophysical Research*, v. 89, p. 10,087–10,101, doi:10.1029/JB089iB12p10087.
- Dahlstrom, C.D.A., 1969, Balanced cross sections: *Canadian Journal of Earth Sciences*, v. 6, p. 743–757, doi:10.1139/e69-069.
- Davis, D., and Engelder, T., 1985, The role of salt in fold-and-thrust belts: *Tectonophysics*, v. 119, p. 67–88, doi:10.1016/0040-1951(85)90033-2.
- Davis, D., Suppe, J., and Dahlen, F.A., 1983, Mechanics of fold-and-thrust belts and accretionary wedges: *Journal of Geophysical Research*, v. 88, p. 1153–1172, doi:10.1029/JB088iB02p01153.
- DeCelles, P.G., 1994, Late Cretaceous–Paleocene synorogenic sedimentation and kinematic history of the Sevier thrust belt, northeast Utah and southwest Wyoming: *Geological Society of America Bulletin*, v. 106, p. 32–56, doi:10.1130/0016-7606(1994)106<0032:LCPSSA>2.3.CO;2.
- DeCelles, P.G., 2004, Late Jurassic to Eocene evolution of the Cordilleran thrust belt and foreland basin system, western USA: *American Journal of Science*, v. 304, p. 105–168, doi:10.2475/ajs.304.2.105.
- DeCelles, P.G., 2012, Foreland basin systems revisited: Variations in response to tectonic setting, in Busby, C., and Azor, A., eds., *Tectonics of Sedimentary Basins: Recent Advances*: Chichester, UK, Blackwell Publishing, p. 405–426, doi:10.1002/9781444347166.ch20.
- DeCelles, P.G., and Coogan, J.C., 2006, Regional structure and kinematic history of the Sevier fold-and-thrust belt, central Utah: *Geological Society of America Bulletin*, v. 118, p. 841–864, doi:10.1130/B25759.1.
- DeCelles, P.G., and Giles, K.N., 1996, Foreland basin systems: *Basin Research*, v. 8, p. 105–123, doi:10.1046/j.1365-2117.1996.01491.x.
- DeCelles, G., and Horton, B.K., 2003, Early to middle Tertiary foreland basin development and the history of Andean crustal shortening in Bolivia: *Geological Society of America Bulletin*, v. 115, p. 58–77, doi:10.1130/0016-7606(2003)115<0058:ETMTFB>2.0.CO;2.
- DeCelles, P.G., and Mitra, G., 1995, History of the Sevier orogenic wedge in terms of critical taper models, northeast Utah and southwest Wyoming: *Geological Society of America Bulletin*, v. 107, p. 454–462, doi:10.1130/0016-7606(1995)107<0454:HOTSOW>2.3.CO;2.
- DeCelles, P.G., Lawton, T.F., and Mitra, G., 1995, Thrust timing, growth of structural culminations, and synorogenic sedimentation in the type area of the Sevier orogenic belt, central Utah: *Geology*, v. 23, p. 699–702, doi:10.1130/0091-7613(1995)023<0699:TTGOSC>2.3.CO;2.
- DeCelles, P.G., Kapp, P., Ding, L., and Gehrels, G.E., 2007, Late Cretaceous to Middle Tertiary basin evolution in the central Tibetan Plateau: Changing environments in response to tectonic partitioning, aridification, and regional elevation gain: *Geological Society of America Bulletin*, v. 119, p. 654–680, doi:10.1130/B26074.1.
- DeCelles, P.G., Ducea, M.N., Kapp, P., and Zandt, G., 2009, Cyclicity in Cordilleran orogenic systems: *Nature Geoscience*, v. 2, p. 251–257, doi:10.1038/ngeo469.
- Densmore, A.L., Ellis, M.A., and Anderson, R.S., 1998, Landsliding and the evolution of normal-fault-bounded mountains: *Journal of Geophysical Research*, ser. B, *Solid Earth and Planets*, v. 103, p. 15,203–15,219, doi:10.1029/98JB00510.
- Dickinson, W.R., 1974, Plate tectonics and sedimentation, in Dickinson, W.R., ed., *Tectonics and Sedimentation*: Society of Economic Paleontologists and Mineralogists (SEPM) Special Publication 22, p. 1–27, doi:10.2110/pec.74.22.0001.
- Dodson, M.H., 1973, Closure temperature in cooling geochronological and petrological systems: *Contributions to Mineralogy and Petrology*, v. 40, p. 259–274, doi:10.1007/BF00373790.
- Dodson, M.H., 1979, Theory of cooling ages, in Jager, E., and Hunziker, J.C., eds., *Lectures in Isotope Geology*: Berlin, Springer-Verlag, p. 194–202, doi:10.1007/978-3-642-67161-6\_14.
- Ehlers, T.A., 2005, Crustal thermal processes and thermochronometer interpretation, in Reiners, P.W., and Ehlers, T.A., eds., *Low-Temperature Thermochronology: Techniques, Interpretations, and Applications*: Mineralogical Society of America, Reviews in Mineralogy and Geochemistry, v. 58, p. 315–350, doi:10.2138/rmg.2005.58.12.
- Ehlers, T.A., and Chapman, D., 1999, Normal fault thermal regimes: conductive and hydrothermal heat transfer surrounding the Wasatch fault, Utah: *Tectonophysics*, v. 312, p. 217–234.

- Ehlers, T.A., and Farley, K.A., 2003, Apatite (U-Th)/He thermochronometry; methods and applications to problems in tectonic and surface processes: *Earth and Planetary Science Letters*, v. 206, p. 1–14, doi:10.1016/S0012-821X(02)01069-5.
- Ehlers, T.A., and Poulsen, C.J., 2009, Influence of Andean uplift on climate and paleoaltimetry estimates: *Earth and Planetary Science Letters*, v. 281, p. 238–248, doi:10.1016/j.epsl.2009.02.026.
- Ehlers, T.A., Farley, K.A., Rasmussen, M.E., and Woodsworth, G.J., 2006, Apatite (U-Th)/He signal of large magnitude and accelerated glacial erosion: Southwest British Columbia: *Geology*, v. 34, p. 765–768, doi:10.1130/G22507.1.
- Elger, K., Oncken, O., and Glodny, J., 2005, Plateau-style accumulation of deformation; southern Altiplano: *Tectonics*, v. 24, TC4020, doi:10.1029/2004TC001675.
- Elliott, D., 1983, The construction of balanced cross sections: *Journal of Structural Geology*, v. 5, p. 101, doi:10.1016/0191-8141(83)90035-4.
- England, P., Le Fort, P., Molnar, P., and Pecher, A., 1992, Heat sources for Tertiary metamorphism and anatexis in the Annapurna-Manaslu region, central Nepal: *Journal of Geophysical Research*, v. 97, p. 2107–2128, doi:10.1029/91JB02272.
- Erdős, Z., van der Beek, P., and Huisman, R.S., 2014, Evaluating balanced section restoration with thermochronology data: A case study from the central Pyrenees: *Tectonics*, v. 33, p. 617–634, doi:10.1002/2013TC003481.
- Erslev, E.A., 1993, Thrusts, back-thrusts and detachment of Rocky Mountain foreland arches, in Schmidt, C.J., Chase, R.B., and Erslev, E.A., eds., *Laramide Basement Deformation in the Rocky Mountain Foreland of the Western United States*: Geological Society of America Special Paper 280, p. 339–358, doi:10.1130/SPE280-p339.
- Erslev, E.A., 2001, Multistage, multidirectional Tertiary shortening and compression in north-central New Mexico: *Geological Society of America Bulletin*, v. 113, p. 63–74, doi:10.1130/0016-7606(2001)113<0063:MMTSAC>2.0.CO;2.
- Farley, K.A., 2000, Helium diffusion from apatite: General behavior as illustrated by Durango fluorapatite: *Journal of Geophysical Research*, v. 105, p. 2903–2914, doi:10.1029/1999JB900348.
- Fitzgerald, P.G., Sorkhabi, R.B., Redfield, T.F., and Stump E., 1995, Uplift and denudation of the central Alaska Range: A case study in the use of apatite fission track thermochronology to determine absolute uplift parameters: *Journal of Geophysical Research*, v. 100, p. 175–20,191.
- Foland, K.A., 1994, Argon diffusion in feldspars, in Parsons, I., ed., *Feldspars and Their Reactions*: Dordrecht, Netherlands, Kluwer, p. 415–447.
- Fosdick, J.C., Grove, M., Hourigan, J.K., and Calderón, M., 2013, Retroarc deformation and exhumation near the end of the Andes, southern Patagonia: *Earth and Planetary Science Letters*, v. 361, p. 504–517, doi:10.1016/j.epsl.2012.12.007.
- Fosdick, J.C., Carrapa, B., and Ortiz, G., 2015, Faulting and erosion in the Argentine Precordillera during changes in subduction regime: Reconciling bedrock cooling and detrital records: *Earth and Planetary Science Letters*, v. 432, p. 73–83, doi:10.1016/j.epsl.2015.09.041.
- Fuller, C.W., Willett, S.D., and Brandon, M.T., 2006a, Formation of forearc basins and their influence on subduction zone earthquakes: *Geology*, v. 34, p. 65–68, doi:10.1130/G21828.1.
- Fuller, C.W., Willett, S., Fisher, D., and Lu, C., 2006b, A thermomechanical wedge model of Taiwan constrained by fission-track thermochronometry: *Tectonophysics*, v. 425, p. 1–24, doi:10.1016/j.tecto.2006.05.018.
- Furlong, K.P., and Edman, J.D., 1984, Graphical approach to the determination of hydrocarbon maturation in overthrust terrains: *American Association of Petroleum Geologists Bulletin*, v. 68, p. 1818–1824.
- Furlong, K.P., and Edman, J.D., 1989, Hydrocarbon maturation in thrust belts; thermal considerations, in Price, R.A., ed., *Origin and Evolution of Sedimentary Basins and Their Energy and Mineral Resources*: American Geophysical Union Geophysical Monograph 48, and International Union of Geodesy and Geophysics Volume 3, p. 137–144.
- Furlong, K.P., Hanson, R.B., and Bowers, J.B., 1991, Modeling thermal regimes: *Reviews in Mineralogy*, v. 26, p. 437–506.
- Gansser, A., 1964, *Geology of the Himalayas*: New York, Wiley-Interscience, 289 p.
- Garzione, C.N., Molnar, P., Libarkin, J., and MacFadden, B., 2006, Rapid late Miocene rise of the Bolivian Altiplano: Evidence for removal of mantle lithosphere: *Earth and Planetary Science Letters*, v. 241, p. 543–556, doi:10.1016/j.epsl.2005.11.026.
- Gillis, R.J., Horton, B.K., and Grove, M., 2006, Thermochronology, geochronology, and upper crustal structure of the Cordillera Real: Implications for Cenozoic exhumation of the central Andean plateau: *Tectonics*, v. 25, TC6007, doi:10.1029/2005TC001887.
- Gilmore, M.E., 2014, *Quantifying Deformation in the Eastern Bhutan Himalaya: Insights from Flexural and Thermal-Kinematic Models of a Balanced Cross Section* [M.S. thesis]: Pittsburgh, Pennsylvania, University of Pittsburgh, 60 p.
- Grove, M., and Harrison, T.M., 1996, <sup>40</sup>Ar\* diffusion in Fe-rich biotite: *The American Mineralogist*, v. 81, p. 940–951, doi:10.2138/am-1996-7-816.
- Grujic, D., Casey, M., Davidson, C., Hollister, L.S., Kuendig, R., Pavlis, T.L., and Schmid, S.M., 1996, Ductile extrusion of the Higher Himalayan crystalline in Bhutan: Evidence from quartz microfabrics: *Tectonophysics*, v. 260, p. 21–43, doi:10.1016/0040-1951(96)00074-1.
- Gurnis, M., 1992, Rapid continental subsidence following the initiation and evolution of subduction: *Science*, v. 255, p. 1556–1558, doi:10.1126/science.255.5051.1556.
- Gurnis, M., 1993, Depressed continental hypsometry behind oceanic trenches: A clue to subduction controls on sea-level change: *Geology*, v. 21, p. 29–32, doi:10.1130/0091-7613(1993)021<0029:DCHBOT>2.3.CO;2.
- Gwinn, V.E., 1970, Kinematic patterns and estimates of lateral shortening, Valley and Ridge and Great Valley Provinces, central Appalachian, south-central Pennsylvania, in Fisher, G.W., et al., eds., *Studies of Appalachian Geology: Central and Southern New York*: New York, Interscience Publishers, p. 127–146.
- Haenel, R., Rybach, L., and Stegena, L., 1988, *Handbook of Terrestrial Heat-Flow Density Determination; with Guidelines and Recommendations of the International Heat Flow Commission*: Dordrecht, Netherlands, Kluwer-Academic, 486 p.
- Hames, W.E., and Bowering, S.A., 1994, An empirical evaluation of the argon diffusion geometry in muscovite: *Earth and Planetary Science Letters*, v. 124, p. 161–169, doi:10.1016/0012-821X(94)00079-4.
- Harrison, T.M., 1982, Diffusion of <sup>40</sup>Ar in hornblende: *Contributions to Mineralogy and Petrology*, v. 78, p. 324–331, doi:10.1007/BF00398927.
- Harrison, T.M., Duncan, I., and McDougall, I., 1985, Diffusion of <sup>40</sup>Ar in biotite: Temperature, pressure and compositional effects: *Geochimica et Cosmochimica Acta*, v. 49, p. 2461–2468, doi:10.1016/0016-7037(85)90246-7.
- Hatcher, R.D., Jr., 1989, Tectonic synthesis of the U.S. Appalachians, in Hatcher, R.D., Jr., et al., eds., *The Appalachian-Ouachita Orogen in the United States*: Boulder, Colorado, Geological Society of America, *Geology of North America*, v. F-2, p. 275–288.
- Hatcher, R.D., Jr., 2004, Properties of thrusts and the upper bounds for the size of thrust sheets, in McClay, K.R., ed., *Thrust Tectonics and Hydrocarbon Systems*: American Association of Petroleum Geologists Memoir 82, p. 18–29.
- Hatcher, R.D., Jr., and Hooper, R.J., 1992, Evolution of crystalline thrust sheets in the internal parts of mountain chains, in McClay, K.R., ed., *Thrust Tectonics*: London, Chapman and Hall, p. 217–233, doi:10.1007/978-94-011-3066-0\_20.
- Henry, P., LePichon, X., and Goffé, B., 1997, Kinematic, thermal and petrological model of the Himalayas: Constraints related to metamorphism within the underthrust Indian crust and topographic evolution: *Tectonophysics*, v. 273, p. 31–56, doi:10.1016/S0040-1951(96)00287-9.
- Henry, S.G., and Pollack, H.N., 1988, Terrestrial heat flow above the Andean subduction zone in Bolivia and Peru: *Journal of Geophysical Research*, v. 93, no. B12, p. 15,153–15,162, doi:10.1029/JB093iB12p15153.
- Herman, F., Copeland, P., Avouac, J.P., Bollinger, L., Maheo, G., Le Fort, P., Rai, S., Foster, D., Pecher, A., Stuwe, K., and Henry, P., 2010, Exhumation, crustal deformation, and thermal structure of the Nepal Himalaya derived from the inversion of thermochronological and thermobarometric data and modeling of the topography: *Journal of Geophysical Research*, v. 115, B06407, doi:10.1029/2008JB006126.
- Herman, F., Seward, D., Valla, P.G., Carter, A., Kohn, B., Willett, S.D., and Ehlers, T.A., 2013, Worldwide acceleration of mountain erosion under a cooling climate: *Nature*, v. 504, p. 423–426, doi:10.1038/nature12877.
- Hilley, G.E., and Strecker, M.R., 2005, Processes of oscillatory basin filling and excavation in a tectonically active orogen: Quebrada del Toro Basin, NW Argentina: *Geological Society of America Bulletin*, v. 117, p. 887–901, doi:10.1130/B25602.1.
- Hodges, K.V., 2000, Tectonics of the Himalaya and southern Tibet from two perspectives: *Geological Society of America Bulletin*, v. 112, p. 324–350, doi:10.1130/0016-7606(2000)112<324:TOTHAS>2.0.CO;2.
- Hodges, K., 2003, Geochronology and thermochronology in orogenic systems, in Turekian, K.K., and Holland, H.D., eds., *Treatise on Geochemistry*: Amsterdam, Elsevier, p. 263–292, doi:10.1016/B0-08-043751-6/03024-3.

- Horton, B.K., 1998, Sediment accumulation on top of the Andean orogenic wedge: Oligocene to late Miocene basins of the Eastern Cordillera, southern Bolivia: *Geological Society of America Bulletin*, v. 110, p. 1174–1192, doi:10.1130/0016-7606(1998)110<1174:SAOTOT>2.3.CO;2.
- Horton, B.K., 1999, Erosional control on the geometry and kinematics of thrust belt development in the central Andes: *Tectonics*, v. 18, p. 1292–1304, doi:10.1029/1999TC900051.
- Horton, B.K., and DeCelles, P.G., 1997, The modern foreland basin system adjacent to the Central Andes: *Geology*, v. 25, p. 895–898, doi:10.1130/0091-7613(1997)025<0895:TMFBSA>2.3.CO;2.
- Hoth, S., Adam, J., Kukowshi, N., and Oncken, O., 2006, Influence of erosion on the kinematics of bivergent orogens: Results from scaled sandbox simulations, *in* Willett, S.D., Hovius, N., Brandon, M., and Fisher, D.M., eds., *Tectonics, Climate, and Landscape Evolution: Geological Society of America Special Paper 398*, p. 201–225.
- House, M.A., Wernicke, B.P., and Farley, K.A., 1998, Dating topography of the Sierra Nevada, California, using apatite (U-Th)/He ages: *Nature*, v. 396, p. 66–69, doi:10.1038/23926.
- Huerta, A.D., and Rodgers, D.W., 2006, Constraining rates of thrusting and erosion: Insights from kinematic thermal modeling: *Geology*, v. 34, p. 541–544, doi:10.1130/G22421.1.
- Huerta, A.D., Royden, L.H., and Hodges, K.V., 1996, The interdependence of deformational and thermal processes in mountain belts: *Science*, v. 273, p. 637–639, doi:10.1126/science.273.5275.637.
- Huntington, K.W., Ehlers, T.A., Hodges, K.V., and Whipp, D.M., Jr., 2007, Topography, exhumation pathway, age uncertainties, and the interpretation thermochronometer data: *Tectonics*, v. 26, TC4012, doi:10.1029/2007TC002108.
- Husson, L., and Moretti, I., 2002, Thermal regime of fold and thrust belts—An application to the Bolivian sub-Andean zone: *Tectonophysics*, v. 345, p. 253–280, doi:10.1016/S0040-1951(01)00216-5.
- Insel, N., Ehlers, T.A., Schaller, M., Barnes, J.B., Tawacoli, S., and Poulsen, C.J., 2010, Spatial and temporal variability in denudation across the Bolivian Andes from multiple geochronometers: *Geomorphology*, v. 122, p. 65–77, doi:10.1016/j.geomorph.2010.05.014.
- Jeffery, L.M., Ehlers, T.A., Yanites, B.J., and Poulsen, C.J., 2013, Quantifying the role of paleoclimate and Andean Plateau uplift on river incision: *Journal of Geophysical Research—Earth Surface*, v. 118, p. 852–871, doi:10.1002/jgrf.20055.
- Jeffery, M.L., Yanites, B.J., Poulsen, C.J., and Ehlers, T.A., 2014, Vegetation-precipitation controls on Central Andean topography: *Journal of Geophysical Research—Earth Surface*, v. 119, p. 1354–1375, doi:10.1002/2013JF002919.
- Jordan, T.E., 1981, Thrust loads and foreland basin evolution: Cretaceous, western United States: *American Association of Petroleum Geologists Bulletin*, v. 65, p. 2506–2520.
- Jordan, T.E., and Allmendinger, R.W., 1986, The Sierras Pampeanas of Argentina: A modern analogue of Rocky Mountain foreland deformation: *American Journal of Science*, v. 286, p. 737–764.
- Jordan, T.E., Allmendinger, R.W., Damanti, J.F., and Drake, R.E., 1993, Chronology of motion in a complete thrust belt: The Precordillera, 30–31°S, Andes Mountains: *The Journal of Geology*, v. 101, p. 135–156, doi:10.1086/648213.
- Jordan, T.E., Schlunegger, F., and Cardozo, N., 2001, Unsteady and spatially variable evolution of the Neogene Andean Bermejo foreland basin, Argentina: *Journal of South American Earth Sciences*, v. 14, p. 775–798, doi:10.1016/S0895-9811(01)00072-4.
- Ketcham, R.A., 1996, Distribution of heat producing elements in the upper and middle crust of southern and west-central Arizona: Evidence from the core complexes: *Journal of Geophysical Research*, v. 101, p. 13,611–13,632, doi:10.1029/96JB00664.
- Ketcham, R.A., Donelick, R.A., and Carlson, W.D., 1999, Variability of apatite fission-track annealing kinetics: III. Extrapolation to geological time scales: *The American Mineralogist*, v. 84, p. 1235–1255, doi:10.2138/am-1999-0903.
- Khanal, S., 2014, Structural and Kinematic Evolution of the Himalayan Fold-Thrust Belt, Central Nepal [Ph.D. diss.]: Tuscaloosa, Alabama, University of Alabama, 185 p.
- Kirby, E., and Whipple, K.X., 2012, Expression of active tectonics in erosional landscapes: *Journal of Structural Geology*, v. 44, p. 54–75, doi:10.1016/j.jsg.2012.07.009.
- Kley, J., 1996, Transition from basement-involved to thin-skinned thrusting in the Cordillera Oriental of southern Bolivia: *Tectonics*, v. 15, p. 763–775, doi:10.1029/95TC03868.
- Kley, J., Monaldi, C.R., and Salfity, J.A., 1999, Along-strike segmentation of the Andean foreland; causes and consequences: *Tectonophysics*, v. 301, p. 75–94, doi:10.1016/S0040-1951(98)90223-2.
- Kohn, M.J., 2008, *P-T-t* data from central Nepal support critical taper and repudiate large-scale channel flow of the Greater Himalayan Sequence: *Geological Society of America Bulletin*, v. 120, p. 259–273, doi:10.1130/B26252.1.
- Kohn, M.J., Wieland, M., Parkinson, C.D., and Upreti, B.N., 2004, Miocene faulting at plate tectonic velocity in the Himalaya of central Nepal: *Earth and Planetary Science Letters*, v. 228, p. 299–310, doi:10.1016/j.epsl.2004.10.007.
- Koons, P.O., 1990, The two-sided orogen: Collision and erosion from the sand box to the Southern Alps: *Geology*, v. 18, p. 679–682, doi:10.1130/0091-7613(1990)018<0679:TSOCAE>2.3.CO;2.
- Kutzbach, J.E., Prell, W.L., and Ruddiman, W.F., 1993, Sensitivity of Eurasian climate to surface uplift of the Tibetan Plateau: *The Journal of Geology*, v. 101, p. 177–190, doi:10.1086/648215.
- Lachenbruch, A., 1968, Rapid estimation of the topographic disturbance to superficial thermal gradients: *Reviews of Geophysics*, v. 6, p. 365–400, doi:10.1029/RG006i003p00365.
- Laslett, G.M., Green, P.F., Duddy, I.R., and Gleadow, A.J.W., 1987, Thermal annealing of fission tracks in apatite. 2. A quantitative analysis: *Chemical Geology*, v. 65, p. 1–13, doi:10.1016/0168-9622(87)90057-1.
- Lavé, J., and Avouac, J.P., 2000, Active folding of fluvial terraces across the Siwaliks Hills, Himalayas of central Nepal: *Journal of Geophysical Research*, v. 105, p. 5735–5770, doi:10.1029/1999JB900292.
- Law, R.D., 2014, Deformation thermometry based on quartz *c*-axis fabrics and recrystallization microstructures: A review: *Journal of Structural Geology*, v. 66, p. 129–161, doi:10.1016/j.jsg.2014.05.023.
- Law, R.D., Searle, M.P., and Simpson, R.L., 2004, Strain, deformation temperatures and vorticity of flow at the top of the Greater Himalayan slab, Everest Massif, Tibet: *Journal of the Geological Society of London*, v. 161, p. 305–320, doi:10.1144/0016-764903-047.
- Law, R.D., Stahr, D.W., III, Francis, M.K., Ashley, K.T., Grasemann, B., and Ahmad, T., 2013, Deformation temperatures and flow vorticities near the base of the Greater Himalayan Series, Sutlej Valley and Shimla Klippe, NW India: *Journal of Structural Geology*, v. 54, p. 21–53, doi:10.1016/j.jsg.2013.05.009.
- Lawton, T.F., Talling, P.J., Hobbs, R.S., Trexler, J.H., Jr., Weiss, M.P., and Burbank, D.W., 1993, Structure and stratigraphy of Upper Cretaceous and Paleogene strata (North Horn Formation), eastern San Pitch Mountains, Utah—Sedimentation at the front of the Sevier orogenic belt: *U.S. Geological Survey Bulletin* 1787, p. I11–I133.
- Lease, R.O., and Ehlers, T.A., 2013, Incision into the eastern Andean Plateau during Pliocene cooling: *Science*, v. 341, p. 774–776, doi:10.1126/science.1239132.
- Lees, C.H., 1910, On the isotherms under mountain ranges in radioactive districts: *Proceeding of the Royal Society*, v. 83, p. 339–346.
- LeFort, P., 1975, Himalayas: The collided range, present knowledge of the continental arc: *American Journal of Science*, ser. A, v. 275, p. 1–44.
- Liu, H., McClay, K.R., and Powell, D., 1992, Physical models of thrust wedges, *in* McClay, K.R., ed., *Thrust Tectonics*: London, Chapman & Hall, p. 71–81.
- Livaccari, R.F., 1991, Role of crustal thickening and extensional collapse in the tectonic evolution of the Sevier-Laramide orogeny, western United States: *Geology*, v. 19, p. 1104–1107, doi:10.1130/0091-7613(1991)019<1104:ROCTAE>2.3.CO;2.
- Lock, J., 2007, *Interpreting Low-Temperature Thermochronometric Data in Fold-and-Thrust Belts: An Example from the Western Foothills, Taiwan* [Ph.D. diss.]: Seattle, Washington, University of Washington, 196 p.
- Lock, J., and Willett, S., 2008, Low-temperature thermochronometric ages in fold-and-thrust belts: *Tectonophysics*, v. 456, p. 147–162, doi:10.1016/j.tecto.2008.03.007.
- Long, S.P., McQuarrie, N., Tobgay, T., and Hawthorn, J., 2011a, Quantifying internal strain and deformation temperature in the Eastern Himalaya, Bhutan: Implications for the evolution of strain in thrust sheets: *Journal of Structural Geology*, v. 33, p. 579–608, doi:10.1016/j.jsg.2010.12.011.
- Long, S.P., McQuarrie, N., Tobgay, T., and Grujic, D., 2011b, Geometry and crustal shortening of the Himalayan fold-thrust belt, eastern and central Bhutan: *Geological Society of America Bulletin*, v. 123, p. 1427–1447, doi:10.1130/B30203.1.
- Long, S.P., McQuarrie, N., Tobgay, T., Coutand, I., Cooper, F., Reiners, P., Wartho, J., and Hodges, K., 2012, Variable shortening rates in the Eastern

- Himalayan thrust belt, Bhutan: Insights from multiple thermochronologic and geochronologic datasets tied to kinematic reconstructions: *Tectonics*, v. 31, TC5004, doi:10.1029/2012TC003155.
- Lovera, O.M., Richter, F.M., and Harrison, T.M., 1991, Diffusion domains determined by <sup>39</sup>Ar release during step heating: *Journal of Geophysical Research*, v. 96, p. 2057–2069, doi:10.1029/90JB02217.
- Lovera, O.M., Grove, M., Harrison, T.M., and Mahon, K.I., 1997, Systematic analysis of K-feldspar <sup>40</sup>Ar/<sup>39</sup>Ar step heating results: I. Significance of activation energy determinations: *Geochimica et Cosmochimica Acta*, v. 61, p. 3171–3192.
- Lucaszeu, F., and Le Douran, S., 1985, The blanketing effect of sedimentation in basins formed by extension: A numerical model. Application to the Gulf of Lyon Viking graben: *Earth and Planetary Science Letters*, v. 74, p. 92–102, doi:10.1016/0012-821X(85)90169-4.
- Malavielle, J., 2011, Impact of erosion, sedimentation, and structural heritage on the structure and kinematics of orogenic wedges: Analog models and case studies: *GSA Today*, v. 20, no. 1, p. 4–10, doi:10.1130/GSATG48A.1.
- Mancktelow, N.S., and Graseman, B., 1997, Time dependent effects of heat advection and topography on cooling histories during erosion: *Tectonophysics*, v. 270, p. 167–195, doi:10.1016/S0040-1951(96)00279-X.
- Mareschal, J.-C., and Jaupart, C., 2013, Radiogenic heat production, thermal regime and evolution of continental crust: *Tectonophysics*, v. 609, p. 524–534, doi:10.1016/j.tecto.2012.12.001.
- McCarthy, J., and Scholl, D.W., 1985, Mechanisms of subduction accretion along the central Aleutian Trench: *Geological Society of America Bulletin*, v. 96, p. 691–701, doi:10.1130/0016-7606(1985)96<691:MOSAAT>2.0.CO;2.
- McClay, K.R., 1992, Glossary of thrust tectonic terms, in McClay, K.R., ed., *Thrust Tectonics*: London, Chapman & Hall, p. 419–434, doi:10.1007/978-94-011-3066-0.
- McQuarrie, N., 2002a, The kinematic history of the central Andean fold-thrust belt, Bolivia: Implications for building a high plateau: *Geological Society of America Bulletin*, v. 114, p. 950–963, doi:10.1130/0016-7606(2002)114<0950:TKHOTC>2.0.CO;2.
- McQuarrie, N., 2002b, Initial plate geometry, shortening variations, and evolution of the Bolivian orocline: *Geology*, v. 30, p. 867–870, doi:10.1130/0091-7613(2002)030<0867:IPGSVA>2.0.CO;2.
- McQuarrie, N., and DeCelles, P.G., 2001, Geometry and structural evolution of the central Andean back thrust belt, Bolivia: *Tectonics*, v. 20, p. 669–692, doi:10.1029/2000TC001232.
- McQuarrie, N., and Ehlers, T.A., 2015, Influence of thrust belt geometry and shortening rate on thermochronometer cooling ages: Insights from the Bhutan Himalaya: *Tectonics*, v. 34, no. 6, p. 1055–1079, doi:10.1002/2014TC003783.
- McQuarrie, N., Barnes, J., and Ehlers, T.A., 2008, Geometric, kinematic and erosional history of the central Andean Plateau (15–17°S), northern Bolivia: *Tectonics*, v. 27, TC3007, doi:10.1029/2006TC002054.
- McQuarrie, N., Tobgay, T., Long, S.P., Reiners, P.W., and Cosca, M.A., 2014, Variable exhumation rates and variable displacement rates: Documenting a recent slowing of Himalayan shortening in western Bhutan: *Earth and Planetary Science Letters*, v. 386, p. 161–174, doi:10.1016/j.epsl.2013.10.045.
- Mitra, G., 1997, Evolution of salients in a fold-and-thrust belt: The effects of sedimentary basin geometry, strain distribution and critical taper, in Sengupta, S., ed., *Evolution of Geological Structures in Micro- to Macro-Scales*: London, Chapman and Hall, p. 59–90, doi:10.1007/978-94-011-5870-1\_5.
- Mitra, S., 1986, Duplex structures and imbricate thrust systems: Geometry, structural position and hydrocarbon potential: *American Association of Petroleum Geologists Bulletin*, v. 70, p. 1087–1112.
- Mitrovica, J.X., Beaumont, C., and Jarvis, G.T., 1989, Tilting of continental interiors by the dynamical effects of subduction: *Tectonics*, v. 8, p. 1079–1094, doi:10.1029/TC008i005p01079.
- Molnar, P., and England, P.C., 1990, Temperatures, heat flux, and frictional stress near major thrust faults: *Journal of Geophysical Research*, v. 95, p. 4833–4856, doi:10.1029/JB095iB04p04833.
- Molnar, P., and Stock, J.M., 2009, Slowing of India's convergence with Eurasia since 20 Ma and its implications for Tibetan mantle dynamics: *Tectonics*, v. 28, TC3001, doi:10.1029/2008TC002271.
- Moore, J.C., Mascle, A., Taylor, E., Andrieuff, P., Alvarez, F., Barnes, R., Beck, C., Behrmann, J., Blanc, G., Brown, K., Clark, M., Dolan, J., Fisher, A., Gieskes, J., Hounslow, M., McLellan, P., Moran, K., Ogawa, Y., Sakai, T., Schoemaker, J., Vrolijk, P., Wilkins, R., and Williams, C., 1988, Tectonics and hydrology of the northern Barbados Ridge: Results from Ocean Drilling Program Leg 110: *Geological Society of America Bulletin*, v. 100, p. 1578–1593, doi:10.1130/0016-7606(1988)100<1578:TAHOTN>2.3.CO;2.
- Mora, A., Horton, B.K., Mesa, A., Rubiano, J., Ketcham, R.A., Parra, M., Blanco, V., Garcia, D., and Stockli, D.F., 2010, Migration of Cenozoic deformation in the Eastern Cordillera of Colombia interpreted from fission track results and structural relationships: Implications for petroleum systems: *American Association of Petroleum Geologists Bulletin*, v. 94, p. 1543–1580, doi:10.1306/01051009111.
- Mora, A., Casallas, W., Ketcham, R.A., Gomez, D., Parra, M., Namson, J., Stockli, D., Almendral, A., Robles, W., and Ghorbal, B., 2015, Kinematic restoration of contractional basement structures using thermokinematic models: A key tool for petroleum system modeling: *American Association of Petroleum Geologists Bulletin*, v. 99, p. 1575–1598, doi:10.1306/04281411108.
- Naeser, C.W., and Faul, H., 1969, Fission track annealing in apatite and sphene: *Journal of Geophysical Research*, v. 74, p. 705–710, doi:10.1029/JB074i002p0705.
- Olen, S., Ehlers, T.A., and Densmore, M.S., 2012, Limits to reconstructing paleotopography from thermochronometer data: *Journal of Geophysical Research—Earth Surface*, v. 117, F01024, doi:10.1029/2011/JF001985.
- Ori, G.G., and Friend, P.G., 1984, Sedimentary basins, formed and carried piggyback on active thrust sheets: *Geology*, v. 12, p. 475–478, doi:10.1130/0091-7613(1984)12<475:SBFACP>2.0.CO;2.
- Painter, C.S., Carrapa, B., DeCelles, P.G., Gehrels, G.E., and Thomson, S.N., 2014, Exhumation of the North American Cordillera revealed by multi-dating of Upper Jurassic–Upper Cretaceous foreland basin deposits: *Geological Society of America Bulletin*, v. 126, p. 1439–1464, doi:10.1130/B30999.1.
- Paná, D.I., and van der Pluijm, B.A., 2015, Orogenic pulses in the Alberta Rocky Mountains: Radiometric dating of major faults and comparison with the regional tectono-stratigraphic record: *Geological Society of America Bulletin*, v. 127, p. 480–502, doi:10.1130/B31069.1.
- Pearson, D.M., Kapp, P., DeCelles, P.G., Reiners, P.W., Gehrels, G.E., Ducea, M.N., and Pullen, A., 2013, Influence of pre-Andean crustal structure on Cenozoic thrust belt kinematics and shortening magnitude: Northwestern Argentina: *Geosphere*, v. 9, p. 1766–1782, doi:10.1130/GES00923.1.
- Perez, N.D., and Horton, B.K., 2014, Oligocene–Miocene deformational and depositional history of the Andean hinterland basin in the northern Altiplano plateau, southern Peru: *Tectonics*, v. 33, p. 1819–1847, doi:10.1002/2014TC003647.
- Pivnik, D.A., and Johnson, G.D., 1995, Depositional response to Pliocene–Pleistocene foreland partitioning in northwest Pakistan: *Geological Society of America Bulletin*, v. 107, p. 895–922, doi:10.1130/0016-7606(1995)107<0895:DRTPPF>2.3.CO;2.
- Price, R.A., 1973, Large scale gravitational flow of supercrustal rocks, southern Canadian Rockies, in De Jong, K.A., and Scholten, R., eds., *Gravity and Tectonics*: New York, John Wiley and Sons, p. 491–502.
- Price, R.A., 1981, The Cordilleran Foreland Thrust and Fold Belt in the Southern Canadian Rocky Mountains: *Geological Society, London, Special Publication* 9, 22 p.
- Rahn, M.K., and Grasemann, B., 1999, Fission track and numerical thermal modeling of differential exhumation of the Glarus thrust plane (Switzerland): *Earth and Planetary Science Letters*, v. 169, p. 245–259, doi:10.1016/S0012-821X(99)00078-3.
- Rahn, M.K., Brandon, M.T., Batt, G.E., and Garver, J.I., 2004, A zero-damage model for fission-track annealing in zircon: *The American Mineralogist*, v. 89, p. 473–484, doi:10.2138/am-2004-0401.
- Rak, A.J., 2015, *Geometry, Kinematics, Exhumation and Sedimentation of the Northern Bolivian Fold-Thrust-Belt Foreland Basin System [M.S. thesis]*: Pittsburgh, Pennsylvania, University of Pittsburgh, 121 p.
- Ramos, V.A., Zapata, T., Cristallini, E., and Introcaso, A., 2004, The Andean thrust system—Latitudinal variations in structural style and orogenic shortening, in McClay, K.R., ed., *Thrust Tectonics and Hydrocarbon Systems*: American Association of Petroleum Geologists Memoir 82, p. 30–50.
- Reiners, P.W., 2005, Zircon (U-Th)/He thermochronometry, in Reiners, P.W., and Ehlers, T.A., eds., *Low-Temperature Thermochronology: Techniques, Interpretations, and Applications*: Mineralogical Society of America, Reviews in Mineralogy and Geochemistry, v. 58, p. 151–179.
- Reiners, P.W., and Brandon, M.T., 2006, Using thermochronology to understand orogenic erosion: *Annual Review of Earth and Planetary Sciences*, v. 34, p. 419–466, doi:10.1146/annurev.earth.34.031405.125202.

- Reiners, P.W., and Ehlers, T.A., eds., 2005, Low-Temperature Thermochronology: Techniques, Interpretations, and Applications: Mineralogical Society of America, Reviews in Mineralogy and Geochemistry, v. 58, 622 p.
- Reiners, P.W., and Farley, K.A., 1999, He diffusion and (U-Th)/He thermochronometry of titanite: *Geochimica et Cosmochimica Acta*, v. 63, p. 3845–3859, doi:10.1016/S0016-7037(99)00170-2.
- Reiners, P.W., Brady, R., Farley, K.A., Fryxell, J.E., Weirnicke, B., and Lux, D., 2000, Helium and argon thermochronometry of the Gold Butte block, south Virgin Mountains, Nevada: *Earth and Planetary Science Letters*, v. 178, p. 315–326, doi:10.1016/S0012-821X(00)00080-7.
- Reiners, P.W., Spell, T.L., Nicolescu, S., and Zanetti, K.A., 2004, Zircon (U-Th)/He thermochronometry: He diffusion and comparisons with  $^{40}\text{Ar}/^{39}\text{Ar}$  dating: *Geochimica et Cosmochimica Acta*, v. 68, p. 1857–1887, doi:10.1016/j.gca.2003.10.021.
- Reiners, P.W., Thomson, S.N., Vernon, A., Willett, S.D., Zattin, M., Einhorn, J., Gehrels, G., Quade, J., Pearson, D.M., Murray, K.E., and Cavazza, W., 2015, Low-temperature thermochronologic trends across the central Andes, 21°S–28°S, in DeCelles, P.G., Ducea, M.N., Carrapa, B., and Kapp, P.A., eds., *Geodynamics of a Cordilleran Orogenic System: The Central Andes of Argentina and Northern Chile*: Geological Society of America Memoir 212, p. 215–249, doi:10.1130/2015.1212(12).
- Rich, J.L., 1934, Mechanics of low angle overthrust faulting illustrated by the Cumberland thrust block, Virginia: *American Association of Petroleum Geologists Bulletin*, v. 18, p. 1584–1596.
- Robbins, G.A., 1972, Radiogenic Argon Diffusion in Muscovite under Hydrothermal Conditions [M.S. thesis]: Providence, Rhode Island, Brown University, 42 p.
- Robert, X., van der Beek, P., Braun, J., Perry, C., and Mugnier, J.-L., 2011, Control of detachment geometry on lateral variations in exhumation rates in the Himalaya: Insights from low-temperature thermochronology and numerical modeling: *Journal of Geophysical Research*, v. 116, B05202, doi:10.1029/2010JB007893.
- Robinson, D.M., 2008, Forward modeling the kinematic sequence of the central Himalayan thrust belt, western Nepal: *Geosphere*, v. 4, p. 785–801, doi:10.1130/GES00163.1.
- Robinson, D.M., and McQuarrie, N., 2012, Pulsed deformation and variable slip rates within the central Himalayan thrust belt: *Lithosphere*, v. 4, p. 449–464, doi:10.1130/L204.1.
- Robinson, D.M., DeCelles, P.G., Garzone, C.N., Pearson, O.N., Harrison, T.M., and Catlos, E.J., 2003, Kinematic model for the Main Central thrust in Nepal: *Geology*, v. 31, p. 359–362, doi:10.1130/0091-7613(2003)031<0359:KMFTMC>2.0.CO;2.
- Robinson, D.M., DeCelles, P.G., and Copeland, P., 2006, Tectonic evolution of the Himalayan thrust belt in western Nepal: Implications for channel flow models: *Geological Society of America Bulletin*, v. 118, p. 865–885, doi:10.1130/B25911.1.
- Rodgers, J., 1950, Mechanics of Appalachian folding as illustrated by Sequatchie anticline Tennessee and Alabama: *American Association of Petroleum Geologists Bulletin*, v. 34, p. 672–681.
- Roeder, D., and Chamberlain, R.L., 1995, Structural geology of Subandean fold and thrust belt in northwestern Bolivia, in Tankard, A.J., Suarez, R., and Welsink, H.J., eds., *Petroleum Basins of South America*: American Association of Petroleum Geologists Memoir 62, p. 459–479.
- Royden, L.H., 1993, The steady-state thermal structure of eroding orogenic belts and accretionary prisms: *Journal of Geophysical Research*, ser. B, Solid Earth and Planets, v. 98, p. 4487–4507, doi:10.1029/92JB01954.
- Royse, F., 1993, Case of the Phantom foredeep: Early Cretaceous in west-central Utah: *Geology*, v. 21, no. 2, p. 133–136, doi:10.1130/0091-7613(1993)021<0133:COTPF>2.3.CO;2.
- Ruppel, C., and Hodges, K.V., 1994, Role of horizontal thermal conduction and finite time thrust emplacement in simulation of pressure-temperature-time paths: *Earth and Planetary Science Letters*, v. 123, p. 49–60, doi:10.1016/0012-821X(94)90256-9.
- Ruppert, L.F., Hower, J.C., Ryder, R.T., Levine, J.R., Trippi, M.H., and Grady, W.C., 2010, Geologic controls on thermal maturity patterns in Pennsylvanian coal-bearing rocks in the Appalachian basin: *International Journal of Coal Geology*, v. 81, p. 169–181, doi:10.1016/j.coal.2009.12.008.
- Safran, E.B., Bierman, P.R., Aalto, R., Dunne, T., Whipple, K.X., and Caffee, M.W., 2005, Erosion rates driven by channel network incision in the Bolivian Andes, in Heimsath, A.M., and Ehlers, T.A., eds., *Quantifying Rates and Timescales of Geomorphic Processes: Part 1: Earth Surface Processes and Landforms*, v. 30, no. 8, special issue, p. 1007–1024, doi:10.1002/esp.1259.
- Safran, E.B., Blythe, A.E., and Dunne, T., 2006, Spatially variable exhumation rates in orogenic belts: An Andean example: *The Journal of Geology*, v. 114, p. 665–681, doi:10.1086/507613.
- Sak, P.B., McQuarrie, N., Oliver, B.P., Lavdovsky, N., and Jackson, M.S., 2012, Unraveling the central Appalachian fold-thrust belt, Pennsylvania: The power of sequentially restored balanced cross sections for a blind fold-thrust belt: *Geosphere*, v. 8, doi:10.1130/GES00676.1, p. 685–702.
- Schelling, D., 1992, The tectonostratigraphy and structure of the eastern Nepal Himalaya: *Tectonics*, v. 11, no. 5, p. 925–943, doi:10.1029/92TC00213.
- Schmidt, C.J., Chase, R.B., and Erslev, E.A., 1993, Laramide Basement Deformation in the Rocky Mountain Foreland of the Western United States: *Geological Society of America Special Paper* 280, 446 p.
- Seidl, M.A., and Dietrich, W.E., 1992, The problem of channel erosion into bedrock: *Catena*, v. 23, supplement, p. 101–124.
- Seidl, M.A., Dietrich, W.E., and Kirchner, J.W., 1994, Longitudinal profile development into bedrock: An analysis of Hawaiian channels: *The Journal of Geology*, v. 102, p. 457–474, doi:10.1086/629686.
- Shaw, J.H., Connors, C., and Suppe, J., 2005, Seismic Interpretation of Contractional Fault-Related Folds: An AAPG Seismic Atlas: *American Association of Petroleum Geologists Studies in Geology* 53, 157 p.
- Shi, Y., and Wang, C., 1987, Two-dimensional modeling of the *P-T-t* paths of regional metamorphism in simple overthrust terrains: *Geology*, v. 15, p. 1048–1051, doi:10.1130/0091-7613(1987)15<1048:TMOTPP>2.0.CO;2.
- Smith, G., McNeill, L., Henstock, T.J., and Bull, J., 2012, The structure and fault activity of the Makran accretionary prism: *Journal of Geophysical Research*, v. 117, B07407, doi:10.1029/2012JB009312.
- Smithson, S.B., Brewer, J., Kaufman, S., Oliver, J., and Hurich, C., 1978, Nature of the Wind River thrust, Wyoming, from COCORP deep-reflection data and from gravity data: *Geology*, v. 6, p. 648–652, doi:10.1130/0091-7613(1978)6<648:NOTWRT>2.0.CO;2.
- Sobel, E.R., and Strecker, M.R., 2003, Uplift, exhumation and precipitation: Tectonic and climatic control of late Cenozoic landscape evolution in the northern Sierras Pampeanas, Argentina: *Basin Research*, v. 15, p. 431–451, doi:10.1046/j.1365-2117.2003.00214.x.
- Sobel, E.R., Hilley, G.E., and Strecker, M.R., 2003, Formation of internally-drained contractional basins by aridity-limited bedrock incision: *Journal of Geophysical Research*, v. 108, B72344, doi:10.1029/2002JB001883.
- Stockli, D.F., Farley, K.A., and Dumitru, T.A., 2000, Calibration of the apatite (U-Th)/He thermochronometer on an exhumed fault block, White Mountains, California: *Geology*, v. 28, p. 983–986, doi:10.1130/0091-7613(2000)28<983:COTAHT>2.0.CO;2.
- Stockmal, G.S., Beaumont, C., Nguyen, M., and Lee, B., 2007, Mechanics of thin-skinned fold-and-thrust belts: Insights from numerical models, in Sears, W.J., Marms, T.A., and Evenchick, C.A., eds., *Whence the Mountains? Inquiries into the Evolution of Orogenic Systems: A Volume in Honor of Raymond A. Price*: *Geologic Society of America Special Paper* 433, p. 63–98, doi:10.1130/2007.2433(04).
- Stolar, D.R., Willett, S.D., and Roe, G.H., 2006, Climatic and tectonic forcing of a critical orogen, in Willett, S.D., Hovius, N., Brandon, M., and Fisher, D.M., eds., *Tectonics, Climate, and Landscape Evolution*: *Geological Society of America Special Paper* 398, *Penrose Conference Series*, p. 241–250.
- Stone, D.S., 1993, Basement-involved thrust-generated folds as seismically imaged in the subsurface of the central Rocky Mountain foreland, in Schmidt, C.J., Chase, R.B., and Erslev, E.A., eds., *Laramide Basement Deformation in the Rocky Mountain Foreland of the Western United States*: *Geological Society of America Special Paper* 280, p. 271–318, doi:10.1130/SPE280-p271.
- Stüwe, K., White, L., and Brown, R., 1994, The influence of eroding topography on steady-state isotherms; application to fission track analysis: *Earth and Planetary Science Letters*, v. 124, p. 63–74, doi:10.1016/0012-821X(94)00068-9.
- Suppe, J., 1983, Geometry and kinematics of fault-bend folding: *American Journal of Science*, v. 283, p. 684–721, doi:10.2475/ajs.283.7.684.
- Suppe, J., 2007, Absolute fault and crustal strength from wedge tapers: *Geology*, v. 35, p. 1127–1130, doi:10.1130/G24053A.1.
- Tagami, T., Galbraith, R.F., Yamada, R., and Laslett, G.M., 1998, Revised annealing kinetics of fission tracks in zircon and geological implications, in Van den haute, P., and De Corte, F., eds., *Advances in Fission-Track Geochronology*: Dordrecht, Netherlands, Kluwer Academic Publishers, p. 99–112.

- Taira, A., Hill, I., Firth, J., Berner, U., Brückmann, W., Byrne, T., Chabernaud, T., Fisher, A., Foucher, J.-P., Gamoto, T., Gieskes, J., Hyndman, R., Karig, D., Kastner, M., Kato, Y., Lallemand, S., Lu, R., Maltman, A., Moore, G., Moran, K., Olafsson, G., Owens, W., Pickering, K., Siena, F., Taylor, E., Underwood, M., Wilkinson, C., Yamano, M., and Zhang, J., 1992, Sediment deformation and hydrogeology of the Nankai Trough accretionary prism: Synthesis of shipboard results of ODP Leg 131: *Earth and Planetary Science Letters*, v. 109, p. 431–450, doi:10.1016/0012-821X(92)90104-4.
- ter Voorde, M., de Bruijne, C.H., Cloetingh, S.A.P.L., and Andriessen, P.A.M., 2004, Thermal consequences of thrust faulting: Simultaneous versus successive fault activation and exhumation: *Earth and Planetary Science Letters*, v. 223, p. 395–413, doi:10.1016/j.epsl.2004.04.026.
- Theissen, S., and Rüpke, L.H., 2009, Feedbacks of sedimentation on crustal heat flow: New insights from the Vøring Basin, Norwegian Sea: *Basin Research*, v. 22, p. 976–990, doi:10.1111/j.1365-2117.2009.00437.x.
- Thiede, R.C., and Ehlers, T.A., 2013, Large spatial and temporal variations in Himalayan denudation: *Earth and Planetary Science Letters*, v. 371–372, p. 278–293, doi:10.1016/j.epsl.2013.03.004.
- Thiede, R.C., Ehlers, T.A., Bookhagen, B., and Strecker, M.R., 2009, Erosional variability along the northwest Himalayan front: *Journal of Geophysical Research*, v. 114, F01015, doi:10.1029/2008JF001010.
- Thomas, W.A., 1977, Evolution of the Appalachian–Ouachita salients and recesses from reentrants and promontories in the continental margin: *American Journal of Science*, v. 277, p. 1233–1278, doi:10.2475/ajs.277.10.1233.
- Thomson, S.N., Brandon, M.T., Reiners, P.W., Zattin, M., Isaacson, P.J., and Balestrieri, M.L., 2010, Thermochronologic evidence for orogen-parallel variability in wedge kinematics during extending convergent orogenesis of the Northern Apennines, Italy: *Geological Society of America Bulletin*, v. 122, p. 1160–1179, doi:10.1130/B26573.1.
- Val, P., Hoke, G.D., Fosdick, J.C., and Wittmann, H., 2016, Reconciling tectonic shortening, sedimentation and spatial patterns of erosion from <sup>10</sup>Be paleo-erosion rates in the Argentine Precordillera: *Earth and Planetary Science Letters*, v. 450, p. 173–185, doi:10.1016/j.epsl.2016.06.015.
- van der Velden, A.J., and Cook, F.A., 1994, Displacement of the Lewis thrust sheet in southwestern Canada: New evidence from seismic reflection data: *Geology*, v. 22, p. 819–822, doi:10.1130/0091-7613(1994)022<0819:DOTLTS>2.3.CO;2.
- Vannucchi, P., Morgan, J.P., Silver, E.A., and Kluesner, J.W., 2016, Origin and dynamics of depositional subduction margins: *Geochemistry Geophysics Geosystems*, v. 17, p. 1966–1974, doi:10.1002/2016GC006259.
- von Huene, R., and Scholl, D.W., 1991, Observations at convergent margins concerning sediment subduction, subduction erosion, and the growth of continental crust: *Reviews of Geophysics*, v. 29, p. 279–316, doi:10.1029/91RG00969.
- von Huene, R., Ranero, C.R., and Vannucchi, P., 2004, Generic model of subduction erosion: *Geology*, v. 32, p. 913–916, doi:10.1130/G20563.1.
- Wagner, G.A., and Reimer, G.M., 1972, Fission track tectonics: The tectonic interpretation of fission track ages: *Earth and Planetary Science Letters*, v. 14, p. 263–268, doi:10.1016/0012-821X(72)90018-0.
- Watt, S., and Durrani, S.A., 1985, Thermal stability of fission tracks in apatite and sphene: Using confined-track-length measurements: *Nuclear Tracks*, v. 10, p. 349–357.
- Webb, A.A.G., 2013, Preliminary palinspastic reconstruction of Cenozoic deformation across the Himalachal Himalaya (northwestern India): *Geosphere*, v. 9, p. 572–587, doi:10.1130/GES00787.1.
- Whipp, D.M., and Ehlers, T.A., 2007, Influence of groundwater flow on thermochronometer-derived exhumation rates in the central Nepalese Himalaya: *Geology*, v. 35, p. 851–854, doi:10.1130/G23788A.1.
- Whipp, D.M., Ehlers, T.A., Blythe, A.E., Huntington, K.W., Hodges, K.V., and Burbank, D.W., 2007, Plio-Quaternary exhumation history of the central Nepalese Himalaya: 2. Thermokinematic and thermochronometer age prediction model: *Tectonics*, v. 26, TC3003, doi:10.1029/2006TC001991.
- Whipp, D.M., Ehlers, T.A., Braun, J., and Spath, C.D., 2009, Effects of exhumation kinematics and topographic evolution on detrital thermochronometer data: *Journal of Geophysical Research—Earth Surface*, v. 114, F04021, doi:10.1029/2008JF001195.
- Whipple, K.X., and Gasparini, N.M., 2014, Tectonic control of topography, rainfall patterns, and erosion during rapid post-12 Ma uplift of the Bolivian Andes: *Lithosphere*, v. 6, p. 251–268, doi:10.1130/L325.1.
- Whipple, K.X., and Meade, B.J., 2004, Controls on the strength of coupling among climate, erosion, and deformation in two-sided frictional orogenic wedges at steady state: *Journal of Geophysical Research*, v. 109, F01011, doi:10.1029/2003JF000019.
- Whipple, K.X., and Meade, B.J., 2006, Orogen response to changes in climatic and tectonic forcing: *Earth and Planetary Science Letters*, v. 243, p. 218–228, doi:10.1016/j.epsl.2005.12.022.
- Whipple, K., and Tucker, G.E., 1999, Dynamics of the stream-power river incision model; implications for height limits of mountain ranges, landscape response timescales, and research needs: *Journal of Geophysical Research*, v. 104, p. 17,661–17,674, doi:10.1029/1999JB900120.
- Whynot, N., Grujic, D., Long, S.P., and McQuarrie, N., 2010, Apparent temperature gradient across the Lesser Himalayan Sequence: Raman spectroscopy on carbonaceous material in the eastern Bhutan Himalaya, in Leech, M.L., Klemperer, S.L., and Mooney, W.D., eds., *Proceedings for the 25th Himalaya-Karakoram Tibet Workshop*: U.S. Geological Survey Open-File Report 2010-1099, 2 p. [Available at <http://pubs.usgs.gov/of/2010-1099/whynot/>].
- Willett, S.D., 1999, Orogeny and orography: The effects of erosion on the structure of mountain belts: *Journal of Geophysical Research*, v. 104, p. 28,957–28,981.
- Willett, S.D., and Brandon, M.T., 2002, On steady states in mountain belts: *Geology*, v. 30, p. 175–178, doi:10.1130/0091-7613(2002)030<0175:OSSIMB>2.0.CO;2.
- Willett, S.D., and Schlunegger, F., 2010, The last phase of deposition in the Swiss Molasse Basin: From foredeep to negative-alpha basin: *Basin Research*, v. 22, p. 623–639, doi:10.1111/j.1365-2117.2009.00435.x.
- Willett, S.D., Beaumont, C., and Fullsack, P., 1993, Mechanical model for the tectonics of doubly verging orogens: *Geology*, v. 21, p. 371–374, doi:10.1130/0091-7613(1993)021<0371:MMFTTO>2.3.CO;2.
- Willett, S.D., Slingerland, R., and Hovius, N., 2001, Uplift, shortening and steady state topography in active mountain belts: *American Journal of Science*, v. 301, p. 455–485.
- Wobus, C.W., Hodges, K.V., and Whipple, K.X., 2003, Has focused denudation sustained active thrusting at the Himalayan topographic front?: *Geology*, v. 31, p. 861–864, doi:10.1130/G19730.1.
- Wobus, C.W., Heimsath, A.M., Whipple, K.X., and Hodges, K.V., 2005, Active out-of-sequence thrust faulting in the central Nepalese Himalaya: *Nature*, v. 434, p. 1008–1011, doi:10.1038/nature03499.
- Wobus, C., Whipple, K.X., Kirby, E., Snyder, N., Johnson, J., Spyropoulou, K., Crosby, B., and Sheehan, D., 2006, Tectonics from topography: Procedures, promise, and pitfalls, in Willett, S.D., Hovius, N., Brandon, M., and Fisher, D.M., eds., *Tectonics, Climate, and Landscape Evolution*: Geological Society of America Special Paper 398, Penrose Conference Series, p. 55–74.
- Woodward, N.B., Boyer, S.E., and Suppe, J., 1989, Balanced Geological Cross-Sections: An Essential Technique in Geological Research and Exploration: Washington, D.C., American Geophysical Union, Short Course Geology, v. 6, 132 p.
- Wu, J.E., and McClay, K.R., 2011, Two-dimensional analog modeling of fold and thrust belts: Dynamic interactions with syncontractional sedimentation and erosion, in McClay, K., Shaw, J.H., and Suppe, J., eds., *Thrust Fault–Related Folding*: American Association of Petroleum Geologists Memoir 94, p. 301–333.
- Yanites, B.J., and Ehlers, T.A., 2012, Global climate and tectonic controls on the denudation of glaciated mountains: *Earth and Planetary Science Letters*, v. 325–326, p. 63–75, doi:10.1016/j.epsl.2012.01.030.
- Yonkee, W.A., 1992, Basement-cover relations, Sevier orogenic belt, northern Utah: *Geological Society of America Bulletin*, v. 104, p. 280–302, doi:10.1130/0016-7606(1992)104<0280:BCRSOB>2.3.CO;2.
- Zhao, W.L., Davis, D.M., Dahleen, F.A., and Suppe, J., 1986, Origin of convex accretionary wedges: Evidence from Barbados: *Journal of Geophysical Research*, v. 91, p. 10,246–10,258, doi:10.1029/JB091iB10p10246.